Plant Nano Biology 16 (2026) 100274

Contents lists available at ScienceDirect

Plant Nano Biology

journal homepage: www.journals.elsevier.com/plant-nano-biology

Transcriptomic and metabolic reprogramming of durum wheat under nanoplastic exposure

Benedetta Pizziconi [a,1], Giuliana Bruno [b,1], Samuela Palombieri [b], Vittoria Locato [a], Francesco Sestili [b], Sara Cimini [a,*], Laura De Gara [a]

[a] Department of Science and Technology for Sustainable Development and One-Health, Università CampusBio-Medico di Roma, Via Alvaro del Portillo 21, 00125, Italy
[b] Department of Agriculture and Forest Sciences (DAFNE), University of Tuscia, Via S. Camillo de Lellis, SNC, Viterbo 01100, Italy

ARTICLE INFO

Keywords:
Polystyrene-nanoplastics
Osmotic-stress
Carbohydrates-metabolism
Wheat

ABSTRACT

Polystyrene nanoplastics (PSNPs) in agricultural soils are emerging contaminants, yet their effects on staple crops and the extent to which plants genetic background modulates these responses remain poorly understood. Using molecular and biochemical analyses, we investigated the uptake and translocation of 50 and 100 nm PSNPs in durum wheat seedlings and their short-term effects on physiology, metabolism, and transcriptomic profiles. We compared the wild-type Kronos with MRP3, a TILLING-derived mutant in the *TdMRP3* genes encoding the multidrug resistance–associated protein 3, a vacuolar phytic acid transporter, also known to sequester xenobiotics from the cytosol to direct them in the vacuoles. PSNPs penetrated roots and were translocated to shoots in both genotypes. In Kronos, exposure to PSNPs stimulated growth, photosynthetic performance, and carbohydrate mobilization, indicating adaptive metabolic reprogramming. Transcriptomic profiling revealed enrichment of osmotic stress related pathways, including upregulation of aquaporin genes and glycolytic routes, supporting water balance and energy homeostasis. Conversely, MRP3 showed growth reduction, increased lipid peroxidation, proline accumulation, and transcriptional repression of photosynthesis-related genes, reflecting a reduced capacity to cope with stress induced by PSNPs. These results demonstrate a key role for *TdMRP3* in mitigating the effects of PSNPs in durum wheat, likely by enhancing sequestration of PSNPs into vacuoles. By contrast, mutations in this transporter may favor accumulation of PSNPs in the cytosol, exacerbating stress and impairing cellular functions. Although Kronos adapts to PSNPs in the short term, reduced transpiration and gas exchange suggest that this response may be unsustainable over longer exposures. This study provides the first genotype-dependent, multi-omics analysis of durum wheat responses to PSNPs exposure, identifying early signatures associated with short-term tolerance or susceptibility that are directly relevant for the environmental risks assessment of PSNPs contamination in agroecosystems.

1. Introduction

The increasing use of treated wastewater and biosolids in agriculture has raised significant concerns regarding the environmental dissemination of nanoplastics (NPs) from different plastic polymers, all of which have different physiochemical properties explicating diverse outcomes on living organisms. Additionally, since polystyrene is one of the most dispersed plastic polymers in the environment and hard to recycle, which traces were even found in air (Pizziconi et al., 2025), this work solely focused on polystyrene nanoplastics (PSNPs), which are now recognized as emerging soil contaminants (Gong et al., 2021; Kik et al., 2020; Mohanaetal.,2021; Siddiqui et al., 2023). Due to their small size chemical instability, and non-biodegradable nature, PSNPs can persist in the rhizosphere, accumulate in soil matrices, and be readily taken up by plant roots, with potential consequences on plant physiology (Lianetal., 2021;Spanòetal.,2022;Suetal.,2024).While considerable effort has been devoted to understanding the ecotoxicological effects on PSNPs in aquatic ecosystems (Lianetal.,2020;Luoetal.,2023;Sunetal.,2020), knowledge of their impact on agroecosystems, especially in terms of staple crops physiological and metabolic adaptations and stress responses, remains largely underexplored. For instance, the existing literature on PSNPs in aquatic systems documents their widespread

* Corresponding author.
E-mail address: s.cimini@unicampus.it (S. Cimini).
[1] These authors share first authorship.

https://doi.org/10.1016/j.plana.2026.100274
Received 13 November 2025; Received in revised form 26 February 2026; Accepted 10 March 2026
Available online 12 March 2026

presence in surface waters, sediments, and aquatic organisms, with concentrations ranging from 1×10^{-9}μg/mL to approximately 1.2 μg/mL (Saputra et al., 2025b). Additionally, Saputra and co-authors demonstrated that PSNPs act as endocrine disruptors in zebrafish, causing dopaminergic dysfunction, reducing neuronal area and locomotor activity, and increasing anxiety-like behaviors (Saputra et al., 2025c). Morphological studies on zebrafish embryos further revealed that PSNPs exposure impairs visual function and behavior, while vitamin E supplementation could mitigate these negative effects (Saputra et al., 2025a). Regarding terrestrial plants, the effects of PSNPs on staple crops were recently reviewed by Pizziconi et al., (2025), who highlighted the limited number of available studies. Overall, PSNPs have been shown to enter plant tissues and induce oxidative stress; however, bread wheat appears to be among the most tolerant species studied, capable to maintain normal growth despite exposure (Pizziconi et al., 2025). In contrast, the model plant *Arabidopsis thaliana*, displayed significant physiological and molecular alterations, including water depletion, changes in the expression of stress-responsive genes, and accumulation of PSNPs in multiple root compartments, such as the stele and vascular system (Sun et al., 2020; Xiao et al., 2022; Pizziconi et al., 2025).

Durum wheat (*Triticum turgidum L.*) is a crop of major economic and nutritional importance, significantly contributing to local food security in various arid and semi-arid regions around the globe (Ciudad-Mulero et al., 2020). Although the plant's responses to several abiotic stressors, such as drought and heat, or soil contaminants, like heavy metals, have been widely characterized, its interaction with PSNPs is poorly understood (Grosse-Heilmann et al., 2024). PSNPs may interfere with water transport and membrane integrity, potentially inducing osmotic stress conditions mimicking drought (Adamczyk et al.,2023;Kimetal.,2019; Zhouetal.,2020; Lianetal.,2021). These stress conditions often trigger substantial transcriptional and metabolic reprogramming, yet the extent and specificity of these responses in durum wheat remain unexplored.

To investigate the short-term impact of PSNPs on durum wheat physiology and stress adaptation, we employed a comparative approach using the wild-type cultivar Kronos and its mutant line, MRP3, which carries a loss-of-function mutation in the *multidrug resistance-associated Protein 3* (*Tdmrp3*) gene, a vacuolar transporter implicated in phytic acid transport and accumulation within the vacuoles and ion homeostasis (Frittellietal.,2023). The MRP3 mutant exhibits a different root architecture, with decreased number of root tips, root length, volume and surface area, and increased root diameter (Frittellietal.,2023). These traits, combined with its altered solute transport capacity, provide an interesting physiological background to assess the impact of PSNPs on conditions of modified intracellular homeostasis. In this study, we exposed Kronos and MRP3 seedlings at an early developmental stage (3 weeks) to two PSNPs size classes (50 and 100 nm) and assessed plant performance through an integrated approach combining phenotypic, physiological and metabolic analyses with transcriptomic profiling.

We aimed to identify early molecular signatures and stress responsive pathways associated with durum wheat seedlings PSNPs exposure, with particular emphasis on osmotic stress-related responses and the associated metabolic reprogramming. By leveraging the comparison between the wild-type and mutant genotypes through a multi-omics approach, these insights are essential for evaluating the potential risks of PSNPs contamination in agricultural systems and for identifying traits associated with crop resilience and, possibly, to the exclusion of PSNPs from plant edible tissues. Additionally, with this study we provide the first genotype-dependent, multi-omics analysis of durum wheat responses to PSNPs, delivering pioneering evidence of early physiological, metabolic, and transcriptional signatures providing a mechanistic interpretation, that are directly relevant for the environmental risk assessment of PSNPs contamination in agroecosystems.

2. Materials and methods

2.1. Plant material and growth conditions

Triticum turgidum L. (cv Kronos) was used for all the experiments. Additionally, an ethyl methane sulfonate (EMS) induced mutant derived from Kronos, designed as MRP3 (Frittelli et al.,2023), was included in this study. The MRP3 mutant line carries a mutation in the genes encoding the Multidrug-Resistance MRP3, transporters involved in the accumulation of phytic acid (PA) within the vacuoles of durum wheat cells. Kronos and MRP3 seeds were surface sterilized in a 10% bleach solution for 1 min, followed by five rinses with sterile distilled water. Sterilized seeds were placed in sterile petri dishes and incubated in darkness at 18°C and 60% relative humidity for 5 days. Germinated seedlings were then transferred in hydroponic growing systems containing 1: 10 modified Hoagland solution in accordance with Cimini et al., (2022). A detailed description of the composition of the Hogland solutions is reported Table S1. Germinated seedlings were kept in controlled environment rooms at 22°C: 18°C, day: night, 16 h:8 h, light: dark, 60% relative humidity and 190–250 μmol photons m^{-2} s^{-1} light intensity (Cimini et al., 2022). During the exposure period of 21 days, hydroponic solutions were daily monitored (temperature and pH) and replenished every 5 days with fresh Hogland solution containing 10 mg/L PSNPs to compensate for evaporation losses and maintain constant exposure conditions. The nominal concentration of 10 mg/L was selected in agreement with an existing bread wheat exposure to PSNPs study (Lian et al., 2020), concentration from which authors obtained the most variations in physiological, metabolic, and gene expression parameters. The concentration was intended to provide dose-response mechanistic insights into early responses to PSNPs rather than reproduce field conditions, even considering the lack of data on actual PSNPs concentrations in agricultural fields.

2.2. PSNPs treatment

PSNPs with diameters of 50 nm (Thermo Fisher Scientific, Catalog No. 3050 A) and 100 nm (ThermoFisher Scientific, Catalog No. 3100 A) were used to treat wheat plants.

The particles were selected as exposure materials due to their commercial availability and prior independent characterization in aqueous media, where hydrodynamic size distributions were measured by DLS in water-based suspensions (Wong et al., 2020; Cole et al., 2021), supporting the use of nominal size specifications as starting reference for this study; additionally, calibration certificates and physicochemical specifications were provided directly by the manufacturer.

After germination, seedlings were transferred to hydroponic systems containing Hoagland nutrients solutions supplemented with 50 nm and 100 nm PSNPs at a concentration of 10 mg/L obtained by dilution of the manufacturer's stock solution (1% solid). Before hydroponic solutions contamination, the stock solution was ultra-sonicated in an ultrasonic bath (Elmasonic S30H, Elma Schmidbauer GmbH, Singen, Germany) at room temperature for 10 min following the description by Lian et al. (2020). Plants were grown for 21 days. At least three independent experiments were performed for each assay. The exposure duration was selected in agreement with other works to investigate the short-term exposure of durum wheat to PSNPs, to underline early responses to PSNPs and early markers of eventual PSNPs-induced damage (Lian et al., 2020). Understanding how seedlings respond to PSNPs exposure in a controlled environment such as hydroponic systems, may be critical to mitigate the long-term impacts of PSNPs on durum wheat adult plants in realistic environmental scenarios.

2.3. Phenotypic analysis

Phenotypic parameters were measured at the end of the growth period. Leaf growth was assessed by measuring the length of the 3rd

fully expanded leaf. Root growth was evaluated by determining the primary root length. In both cases, analyses were performed using ImageJ software on scanned plant images. Fresh biomass of leaves, roots, and whole seedlings were also recorded. Finally, the number of leaves per seedling was counted. All measurements were performed on a minimum of 3 individual plants per treatment collected from different vessels to ensure statistical robustness and biological independence and to avoid pseudoreplication.

2.4. Imaging by confocal laser scanning microscopy

To investigate the absorption and translocation of PSNPs, Kronos wheat seedlings grown under non-labeled PSNPs treatment for 8 days were transferred to hydroponic systems containing green, fluorescent PSNPs with diameters of 50 nm (Thermo Fisher Scientific, Catalog No. R100B). After 48 h, roots and leaves were collected. Control plants were sampled under the same growth conditions. Roots and leaves samples were collected and analysed using confocal laser scanning microscopy. After collection, roots and leaves were thoroughly washed five times with phosphate-buffered saline (PBS) solution to remove any non-internalized PSNPs adhering to the surface, ensuring that only nanoparticles that had penetrated the tissue were examined. Fresh roots and leaves were directly placed on a glass slide and PBS was added to maintain sample hydration. Samples were analysed using the Eclipse-Ti2 Nikon Laser Scanning Confocal Microscope (Nikon, Japan) using a fluorescein isothiocyanate (FITC) laser with an excitation wavelength of 488 nm. The analysis was conducted using a 10 × magnification objective, and the zoom factor was set to 0.75 to accommodate a larger sample region within the imaging field. For all roots and shoots samples, a Z-stack analysis was performed with a step size of 1 μm, and the scanning mode was set in the XYZ direction with a scan speed of 400 Hz. It is common to observe a certain degree of autofluorescence in plant tissues, particularly in leaves, due to the presence of various pigments and metabolites. To minimize this effect and obtain clearer images, imaging parameters were optimized accordingly. For root samples, high voltage (HV) was set to 50 and gain to 20, whereas for leaf samples, HV was set to 90 and gain to 20. These settings were selected to enhance the signal-to-noise ratio while reducing background interference. Additionally, to further improve image contrast, the “Subtract Background” function was applied to eliminate unwanted light scattering and autofluorescence artifacts. Control samples were analysed under the same microscope settings to ensure reproducibility and comparability across experimental conditions. All imaging analyses were performed in triplicate, with three independent biological replicates for both root and leaf samples. This approach ensured statistical robustness and minimized variability in data interpretation.

2.5. Photosynthetic capacity measurement

Photosynthetic capacity was assessed using a porometer/fluorometer (LI-600, LI-COR, USA) measuring Photosystem II efficiency (PhiPS2), Electron Transport Rate (ETR), transpiration rate per unit leaf area (E) and gas water exchange (gsw) by clamping the second leaf of Kronos and MRP3 plants at different time points and following the standard instrumental procedure described in the manufacturer’s manual (Condò et al., 2025). Measurements were taken 1 h following light exposure.

2.6. Pigments content analysis

The quantification of chlorophyll a, chlorophyll *b* and carotenoids were carried out following the protocol of Lichtenthaler, based on spectrophotometric measurements at specific wavelengths Briefly, 0.2 g of leaf was powdered using liquid nitrogen and homogenized with 80% acetone (Merck KGaA, Darmstadt, Germany) in a 1:5 wt to volume (w: v) ratio. The mixture was then centrifuged at maximum speed, 12,000 xg, for 10 min at 4° C. The supernatant was recovered, and the absorbance was measured by the spectrophotometer UV-1800 Shimidazu, at the peak wavelengths: 663 (chlorophyll a), 646 (chlorophyll *b*), 470 (carotenoids) nm. The results were expressed as μg of pigments per g of dry weight (μg / g DW) (Lichtenthaler,1987).

2.7. Oxidative stress marker

Malondialdehyde (MDA), a by-product of lipid peroxidation, was quantified using a spectrophotometric method according to Zhang and Huang. Leaf material was homogenized in 80% v/v ethanol using mortar and pestle, then centrifuged at 12,000 × g, for 10 min at 4° C. The supernatant was subsequently reacted with thiobarbituric acid (TBA) to form the TBA–MDA complex. Absorbance of TBA–MDA adduct was measured at 440, 532, and 600 nm, using a micro-plate reader (Infinite 200 Pro from Tecan, Crailsheim, Germany)(ZhangandHuang,2013).

2.8. Proline content determination

The content of proline in leaves was determined as follows CarilloandGibon(2011). Leaf samples (approximately 0.2 g) were homogenized in 70% ethanol. The homogenate was filtered, and the filtrate was mixed with an equal volume of acid-ninhydrin solution and glacial acetic acid. The reaction mixture was incubated at 100°C for 1 h and then cooled. The reaction was stopped by adding toluene, and the absorbance of the upper phase was measured at 520 nm using a Shimadzu UV1800 Spectrophotometer. Proline content was quantified using a standard curve prepared with known concentrations of proline and expressed as μmol g^{-1} fresh weight (CarilloandGibon,2011).

2.9. Free sugars and starch content determination

Free sugars (sucrose, glucose, and fructose) and total starch content were quantified using the K-SUFRG 04/18 and K-TSHK 02/22 assay kits (Megazyme, Wicklow, Ireland), following the manufacturer’s instructions.

2.10. Determination of alpha- amylase's activity

Alpha-Amylase activity was assessed according to the method of YaZhangetal.(2024) with minor modifications. Briefly, fresh leaves (0.3 g) were homogenized in 0.02 M phosphate-buffered saline (PBS, pH 5.9) at a 1:4 (w/v) ratio. The homogenate was centrifuged at 8000 rpm for 10 min at 4°C, and 100 μL of the supernatant were carefully recovered. These 100 μL of supernatant were incubated with 1% starch for 5 min. 200 μL of 15.96 M 3,5-dinitrosalicylic acid (DNS) reagent was added to each tube. Samples were then boiled until a color change indicated reaction completion, then cooled to room temperature. Absorbance was recorded at 540 nm using a Shimadzu UV1800 Spectrophotometer (YaZhangetal.,2024).

2.11. Statistical analysis

Plants were grown in independent hydroponic tanks, which were considered the experimental units. For each experimental run, two tanks were assigned to the control treatment and two tanks to the PSNPs treatment. Within each tank, 25 seedlings per genotype were grown under the same treatment conditions. The experiment was repeated in three independent experimental runs conducted at different time points. For statistical analyses, measurements from individual seedlings were averaged per genotype within each tank, and tank means were used as independent biological replicates, thereby avoiding pseudoreplication. Statistical analysis was performed with GraphPad Prism 10.3.1 (GraphPad Software, Inc., San Diego, CA). Data are presented as mean ± standard error of the mean (SEM) of at least three experimental replicates. Pairwise comparisons were always the control vs the 50 nm PSNPs treated group, and the control vs 100 nm PSNPs treated group. To

determine the statistically significant differences among groups, all data were firstly tested for normality with the Shapiro-Wilk test, then subjected to One-way ANOVA test followed by Tukey's post hoc for normal distributions, or T-test for parametric data, or Kruskal-Wallis followed by Dunn's test for non-parametric data. Significance was set at $p < 0.05$.

2.12. RNA extraction and sequencing

RNA extraction and sequencing were only performed under exposure to 50 nm PSNPs since this treatment consistently induced the most pronounced physiological and metabolic alterations, allowing a focused mechanistic investigation of PSNPs induced transcriptional reprogramming in this first durum wheat genotype-comparative study.

Leaf samples from Kronos and MRP3were collected, immediately frozen in liquid nitrogen (N_2) and stored at −80°C until further processing. Total RNA was extracted using the NucleoSpin RNA Plant kit (MACHEREY-NAGEL GmbH & Co. KG.), following the manufacturer's protocol. To eliminate genomic DNA contamination, RNA samples were treated with the DNA-free DNase Kit (Ambion). RNA concentration was assessed with a NanoDrop 2000 spectrophotometer (Thermo Scientific, MA, USA). RNA integrity was measured with the Bioanalyzer 2100 system (Agilent Technologies, CA, USA). Library preparation and sequencing were performed on a NovaSeq 6000 platform (Illumina, San Diego, CA, USA) using paired end reads. Read counts were obtained using the Counts software (v1.5.0-p3), a read counts tool used to quantify gene level expression from aligned RNA-seq reads prior to differential expression analysis and normalized as fragments per kilobase of transcript per million mapped reads (FPKM).

2.12.1. Transcriptome analyses

Differential expression analysis was performed using DESeq2 (v1.20.0) to compare Kronos_PSNPs and MRP3_PSNPs, representing Kronos andMRP3 exposed to 50 nm PSNPs against their respective controls. Based on the physiological and metabolic screening, transcriptomic analyses were focused only on the 50 nm PSNPs treatment, which showed a more coherent and genotype-dependent modulation of responses. Genes with an adjusted P-value (Benjamini-Hochberg correction) ≤ 0.05 and an absolute $\log_2$ fold change ($|\log_2 FC=) \geq 1$ were considered differentially expressed. Enrichment analysis of differentially expressed genes (DEGs) was conducted using the clusterProfiler R package, which corrects gene length bias to ensure accurate results. Gene Ontology (GO) terms were considered significantly enriched if they had an adjusted *p*-value (padj) of less than 0.05. GO analysis classified DEGs into three main categories: biological processes (BP), cellular components (CC), and molecular functions (MF), providing a comprehensive understanding of their roles. The KEGG pathway analysis was also implemented using the clusterProfiler R package to identify statistically enriched pathways. DEGs associated with KEGG pathways were mapped to specific biochemical pathways to uncover significant biological processes affected by the treatment. From the KEGG analysis, targeted pathway diagrams, known as KEGG pathway TAES (Tool for Annotating Enzyme Systems), were constructed to visualize and analyze the metabolic flow of starch and sucrose metabolism. Finally, the Gene Set Enrichment Analysis (GSEA) was performed using the Broad Institute tool, analyzing GO and KEGG datasets to identify enriched gene sets.

3. Results

3.1. Plants phenotyping

As already reported by Frittelli et al. (2023), Kronos and MRP3 showed a different root phenotype, with MRP3 showing a distinct root architecture with shorter and less linear primary root, higher number of lateral ones, of which the insertion angle diverged more significantly from the primary root (Frittelli et al., 2023). In the developmental stage of our analysis (plantlets of 26 days after germination), also the aerial part of the plant showed a different phenotype with leaf insertion angle more obtuse in MRP3 than in Kronos; moreover, the leaves of MRP3 had a more intense green color than those of Kronos (Fig. 1-A, B). PSNPs treatments also had different effects on the two genotypes. Indeed, 50 and 100 nm PSNPs exposure significantly increased Kronos shoot and root length compared to controls (Fig. 1-C). The biomass of the entire plants as well as those of roots and shoots were also increased (Fig. 1-D, E). On the other hand, both 50 and 100 nm PSNPs exposures were ineffective on MRP3 root growth and biomass, while they induced a decrease in shoot length and in the case of 100 nm PSNPs exposure, a decrease in plant biomass (Fig. 1-D, E). The number of leaves was subjected to a significant variation in Kronos in response to the treatments with a significant increase following both the 50 nm and 100 nm PSNPs exposure, while, in agreement with the decrease in biomass, MRP3 showed a reduction in leaves number when treated with the 100 nm PSNPs (Fig. 1-F).

3.2. PSNPs tracing across tissues

Roots and shoots of Kronos and MRP3 seedlings exposed to 50 nm fluorescent PSNPs were analysed by confocal microscope to search for PSNPs presence in different organs. Fluorescent signals displayed as green-fluorescent dots were clearly observed in roots of both Kronos and MRP3 (Fig. 2-B, D). Interestingly, the fluorescent dots had irregular sizes, reaching a diameter of about 25–100 μm. These signals do not correspond to individual PSNPs but are instead interpreted as localized accumulations of fluorescence, potentially arising from PSNPs aggregation or clustering. In this case, confocal imaging therefore provides qualitative information on PSNP-associated fluorescence localization rather than direct evidence of particle size or quantitative uptake. In shoots, clear fluorescent dots due to the presence of fluorescent 50 nm PSNPs were mainly localized within the vascular system of leaves from PSPN-treated Kronos and MRP3 samples (Fig. 2-F, H). The analyses over z-stack planes confirmed PSNPs internalization, rather than superficial absorption. The performed analyses did not allow a quantification of the PSNPs absorbed at root level and transported in the plant aerial part therefore it is not possible to state whether there were differences in the uptake and transport of PSNPs in the two genotypes. However, a higher presence of fluorescent dots was clearer in the roots than in the leaves of both Kronos and MRP3.

3.3. Photosynthetic efficiency and oxidative stress

The photosynthetic capacity of Kronos and MRP3 leaves, evaluated through measurements of PhiPS2, ETR and gsw, showed a diversified response to PSNPs depending on wheat genotype. Indeed, both PhiPS2 and ETR were enhanced by 50 nm and 100 nm PSNPs exposure in Kronos, while it decreased in MRP3 under both treatments compared to controls (Fig. 3-A, B). Gsw decreased in both genotypes exposed to 50 nm PSNPs, while the treatment with 100 nm PSNPs induced an increase of gsw in Kronos and no significant effect in MRP3. (Fig. 3-C). PSNPs size also influenced the transpiration rate: in both genotypes, exposure to the smallest PSNPs (50 nm) resulted in a decrease, whereas exposure to 100 nm PSNPs led to an increase (Fig. 3-D). The levels of photosynthetic pigments were also analysed in the two genotypes. In agreement with the different colour of the leaves of the two genotypes (Fig. 1-A, B), the levels of chlorophylls and carotenoids were at least 2–3 times higher in MRP3 than in Kronos under control conditions (Fig. 3-E, G). In Kronos, chlorophyll a content increased under 50 nm PSNPs treatment, while it was reduced in MRP3 in response to the 100 nm PSNPs exposure (Fig. 3-E). No effect of PSNPs' exposure was observed on chlorophyll *b* in Kronos, whereas it was decreased in MRP3 under 100 nm PSNPs treatment (Fig. 3-F). Moreover, carotenoids increased in Kronos under both treatments and decreased in MRP3 under 100 nm PSNPs exposure (Fig. 3-G).

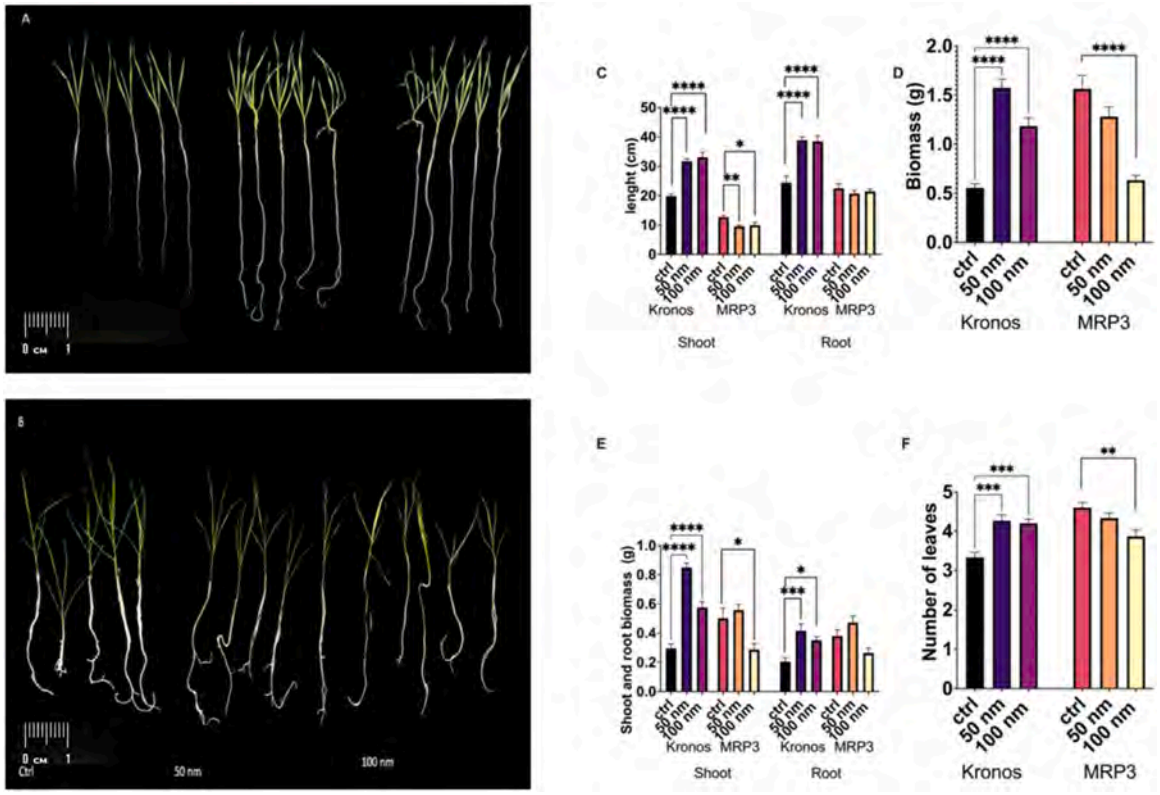

Fig. 1. Kronos (A) and MRP3 (B) seedlings after 21 days under three experimental conditions, from left to right: ctrl, 50 nm PSNPs and 100 nm PSNPs. Effects of 50 nm PSNPs and 100 nm PSNPs on seedlings' shoot and root length (C), expressed as cm. Effects of 50 nm PSNPs and 100 nm PSNPs on seedlings' total biomass (D) and on seedlings' shoot and root biomass (E), expressed as g of fresh weight (FW). Effects of 50 nm and 100 nm PSNPs on the seedlings number of leaves (F). Data are presented as mean ± standard error of the mean (SEM) (n = 15); Tukey's $p < 0.05$ for C, D, E; Dunn's $p < 0.05$ for F. Significant differences among pairwise comparisons are represented with asterisks. (* $p < 0.05$; ** $p < 0.01$; *** $p < 0.001$; **** $p < 0.0001$).

Quantification of MDA was performed in leaves as a marker for lipid peroxidation for addressing PSNPs potential damage to biological membranes. MDA significantly increased in response to 100 nm PSNPs in MRP3 leaves while it did not significantly change in Kronos (Fig. 3-H).

3.4. Transcriptomicreprogramming

Due to the similarity found in the responses to 50 and 100 nm PSNPs exposure in many of the studied parameters, transcriptomic analyses were performed in the leaves of Kronos and MRP3 plants exposed to 50 nm PSNPs and those grown in control condition.

3.4.1. Validation of the analysis and DEGs

A PCA was performed using transcripts per million (TPM) values from three biological replicates for each treatment group. The transcriptomes of the PSNPs-treated Kronos samples **(**WT501, WT502, WT503**)** andMRP3 samples (MRP4, MRP5, MRP6) formed distinct clusters, clearly separating them from their respective controls (WTC1, WTC2, WTC3 for Kronos; MRP1, MRP2, MRP3 for MRP3) (Fig. 4-A). The PCA analysis validated the experimental design and served as quality control, confirming consistency among biological replicates and distinct transcriptional responses to PSNPs treatment. Transcriptomic analysis identified 6622 DEGs in Kronos exposed to PSNPs with 3042 downregulated genes and 3580 upregulated ones (Fig. 4-B). Similarly, in PSNPs treated MRP3**,** 6180 DEGs were identified, comprising 2785 downregulated genes and 3395 upregulated genes (Fig. 4-B). A hierarchical clustering heatmap was generated to visualize the expression patterns of DEGs across experimental conditions. The heatmap highlights similar transcriptional profiles induced by PSNPs exposure for Kronos and MRP3 under PSNPs exposure, with comparable clusters of highly upregulated genes (red) and downregulated genes (green) (Fig. 4-C). Because the expression levels were normalized against each genotype respective control, the columns representing control samples show inverse color patterns relative to their treated counterparts. This contrast highlights the relative magnitude and direction of transcriptional changes induced by PSNPs treatment.

3.4.2. Gene ontology

GO enrichment analysis identified 30 functional subcategories of which terms were significantly enriched in Kronos under 50 nm PSNPs treatment and 30 in MRP3 exposed to 50 nm PSNPs across the three main categories: Biological Process (BP), Molecular Function (MF), and Cellular Component (CC) (Fig. 5-A, B). The Directed Acyclic Graphs (DAG) illustrate the hierarchical relationships among these enriched terms (Fig. 5). The broad parent term response to water (GO:0009415) encompasses multiple, more specific child terms, including response to abiotic stimulus (GO:0009628), to acid chemical (GO:0001101), to inorganic substances (GO:0010035), and to oxygen-containing compounds (GO:1901700) in both genotypes (Fig. 5-A, B). All DEGs annotated under the response to water, abiotic stimulus, acid chemical, inorganic substances and oxygen-containing compounds were related to dehydrin metabolism.

In Kronos under PSNPs treatment, the cellular carbohydrate metabolic process (GO:0044262) and oligosaccharide metabolic process (GO:0009311) were significantly enriched, with disaccharide metabolism representing the broader functional term (GO:0005984). DEGs associated with these GO terms were specifically linked to the metabolism of sucrose, xylose, trehalose, xyloglucan, and callose (Fig. 5-A). In contrast, the treated MRP3 displayed a narrower enrichment profile, with DEGs primary associated with the cellular carbohydrate metabolic process (GO:0044262) (Fig. 5-B). Overall, Kronos displayed a broader transcriptional reprogramming than MRP3 aligned with the enrichment

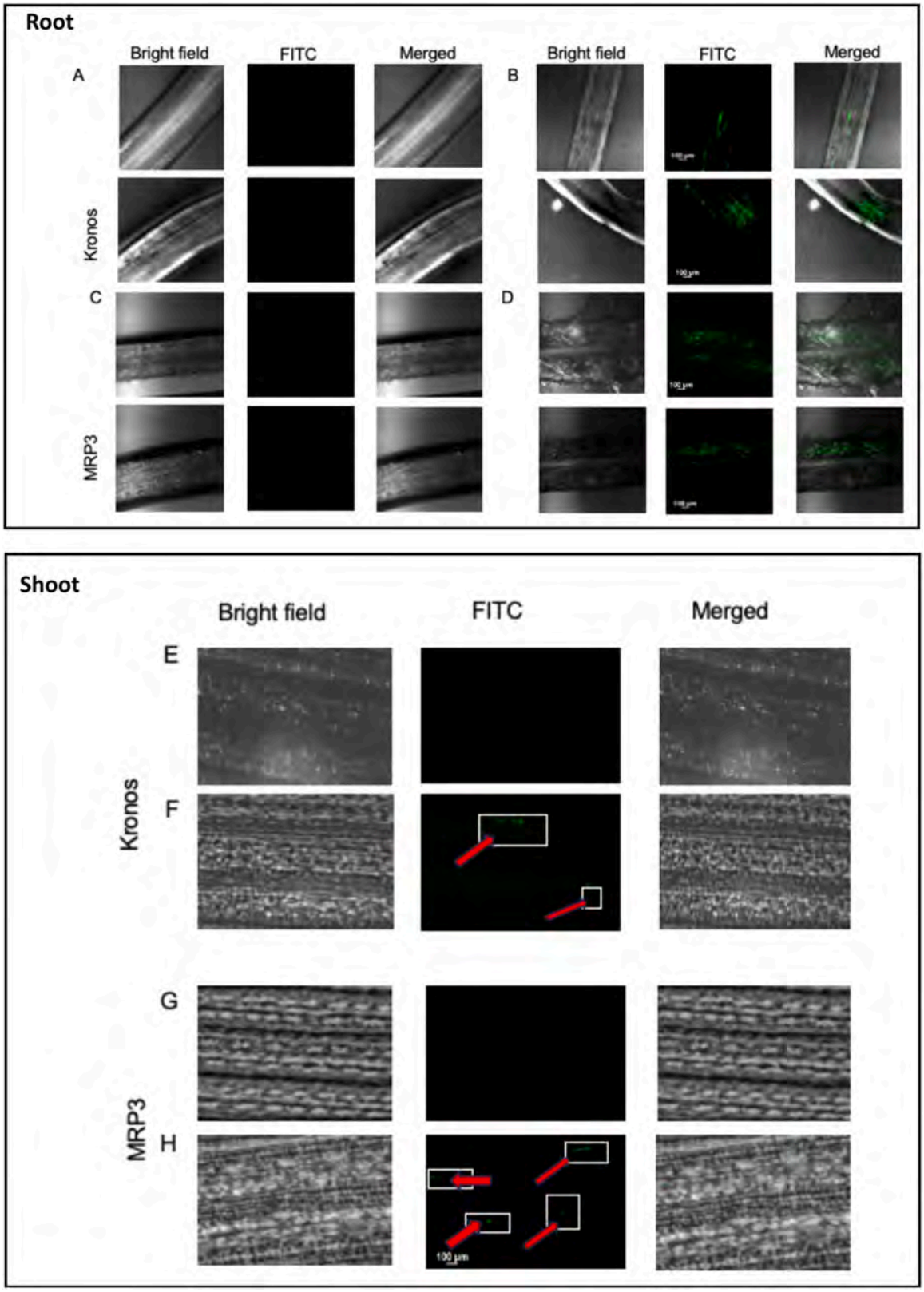

Fig. 2. Confocal images of root segments from Kronos and MRP3. Three different samples of control Kronos (A) and MRP3 (C) roots are shown in comparison with three different samples of Kronos (B) and MRP3 (D) roots from plants treated with 50 nm PSNPs. Each set of images includes bright field (left), FITC fluorescence (middle), and the merged bright field and FITC overlay (right), showing the localization of nanoparticles within plant tissues. Detailed view of PSNPs distribution in leaves from Kronos control (E) compared to Kronos treated with 50 nm PSNPs (F) and MRP3 control (G) compared to MRP3 treated with 50 nm PSNPs (H). The white boxes and red arrows in the FITC channels, highlight the presence of PSNPs inside the leaves. Each set of images includes bright field (left), FITC fluorescence (middle), and the merged bright field and FITC overlay (right), showing the localization of nanoparticles within plant tissues.

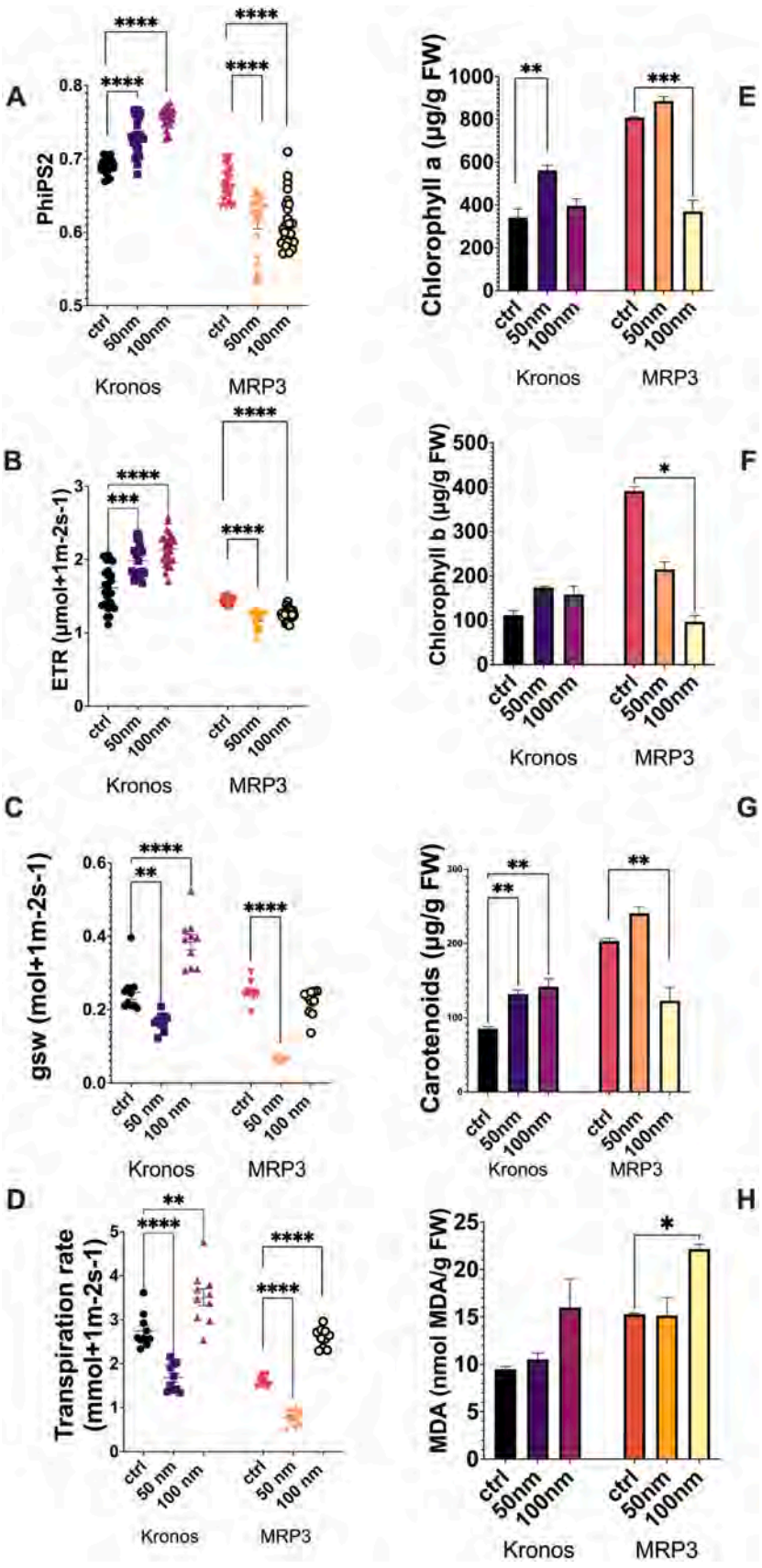

(caption on next page)

Fig. 3. Effects of 50 nm PSNPs and 100 nm PSNPs on PhiPS2 (A), and ETR (B) expressed as $\mu mol^{+1}\ m^{-2}\ s^{-1}$; Transpiration rate (C), described as $\mu mol^{+1}\ m^{-2}\ s^{-1}$; gsw (D), described as $\mu mol^{+1}\ m^{-2}\ s^{-1}$; (n = 15). Effects of 50 nm PSNPs and 100 nm PSNPs on seedlings' chlorophyll a (E), chlorophyll *b* (F) and carotenoids (G). Effects of 50 nm PSNPs and 100 nm PSNPs on MDA content expressed as nmol MDA/g FW (H); (n = 3). Data are presented as mean ± standard error of the mean (SEM); Tukey's $p < 0.05$ for A, C, D, E, G and H; Dunn's $p < 0.05$ for B, F. Significant differences among pairwise comparisons are represented with asterisks (* $p < 0.05$; ** $p < 0.01$; *** $p < 0.001$; **** $p < 0.0001$).

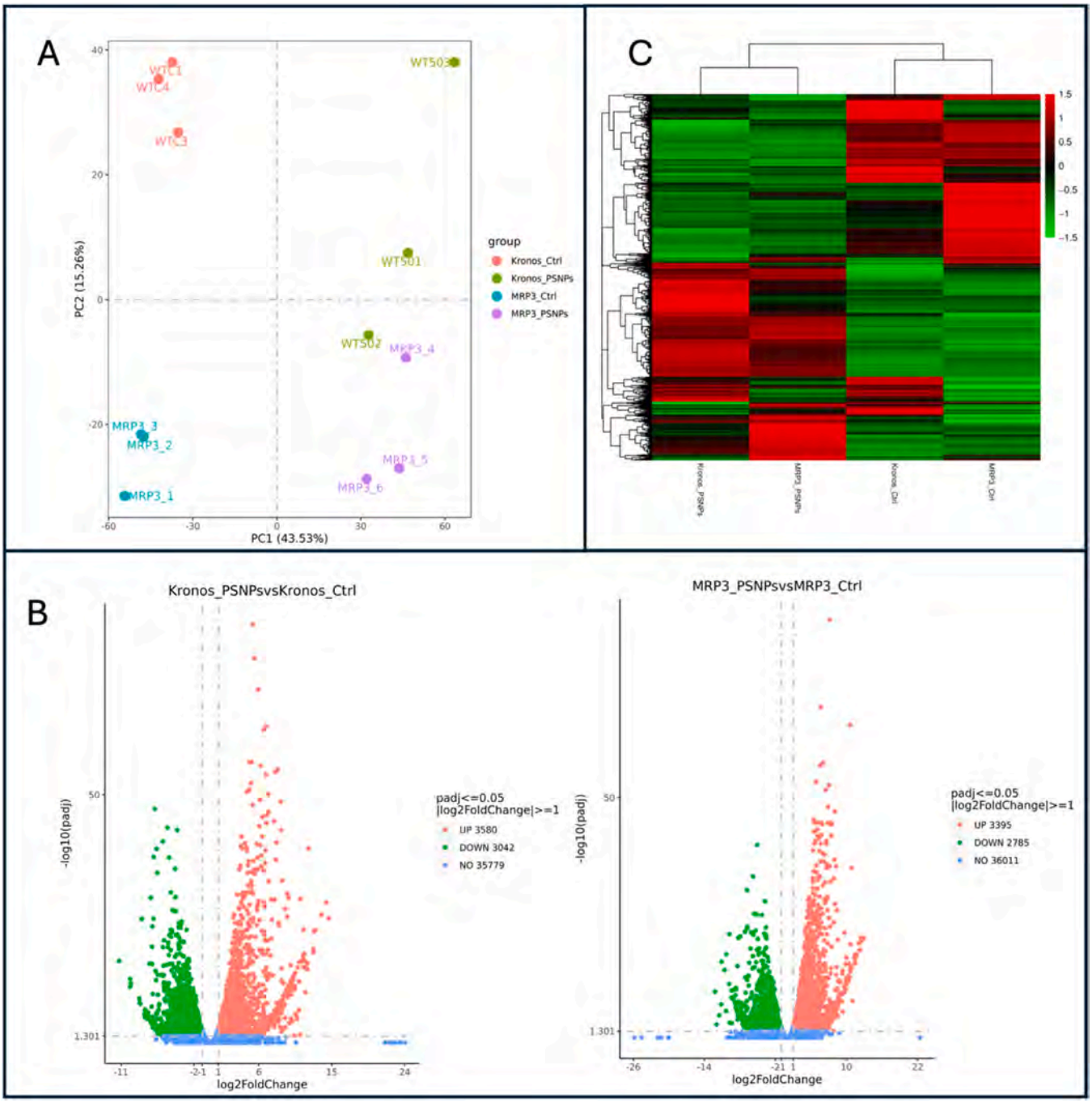

Fig. 4. PCA of the transcriptome of all 3 biological samples based on the normalized count of all genes. Samples scores for the first and second principal component are plotted, with explained percentage of variance of PC1 and PC2 indicated along the x and y axes (A). Volcano plots display genes that are upregulated and downregulated for Kronos_PSNPs and for MRP3_PSNPs (B). Red plots stand for upregulated genes; green dots stand for downregulated genes; Blue dots stand for genes without significant differences of expression. Hierarchical clustering heatmap comparing DEGs in all the experimental conditions (C).

of more specific GO terms.

3.4.3. *Kyoto encyclopedia of genes and genomes enrichment*

KEGG pathway enrichment analysis identified 18 significantly enriched pathways in Kronos exposed to PSNPs and 14 pathways in MRP3 exposed to PSNPs, all with a padj< 0.05. Among these, 8 pathways were commonly enriched between the two 50 nm PSNPs exposed genotypes compared to their controls, indicating shared transcriptional

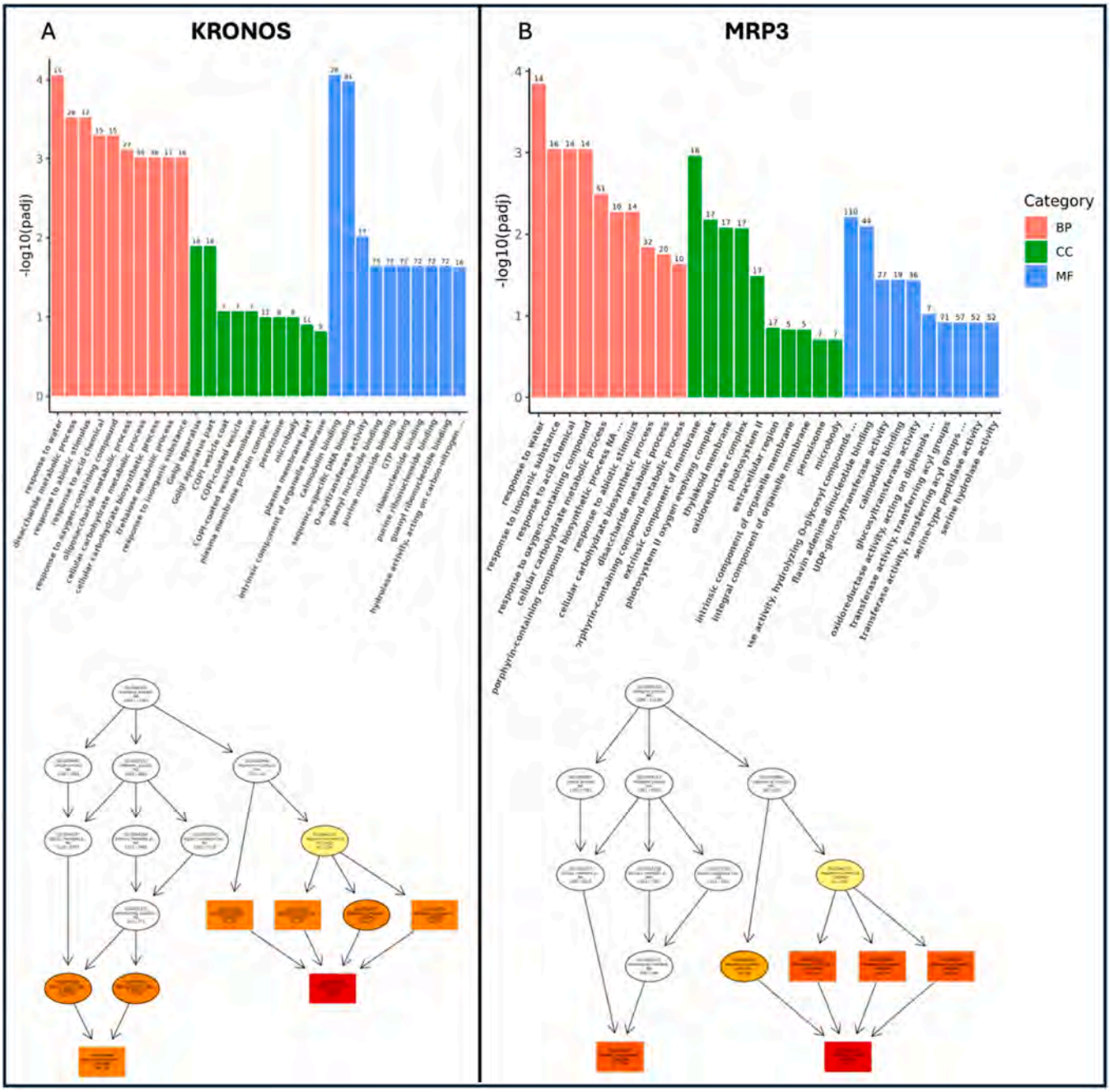

Fig. 5. GO enrichment analysis of DEGs for Kronos_PSNPs and MRP3_PSNPs (A and B). Y axes correspond to -log10 (padj). Higher values indicate greater statistical significance of differential expressions. X axes correspond to the GO terms. Numbers on the bars represent the DEGs count for GO terms. Directed Acyclic Graphs (DAG) showing the hierarchical structure of GO terms under BP category for Kronos_PSNPs and for MRP3_PSNPs (bottom A and B). Each node corresponds to a specific GO term, with arrows representing the relationship between terms. The colors of the nodes represent the padj: orange stands for padj < 0.05, red stands for a much lower padj.

responses due to PSNPs exposure. Treated Kronos exhibited 10 exclusive pathways, reflecting a broader transcriptional reprogramming compared to the 6 significant exclusive pathways in MRP3 under PSNPs exposure, which exhibited a more targeted transcriptional response (Fig. 6-A). Through the commonly enriched pathways, plant hormone signal transduction (ko04075) emerged as the most enriched in both genotypes. It involved DEGs for signaling molecules such as auxins, gibberellins, and abscisic acid, which regulate stress responses and growth. Kronos exposed to the treatment, exhibited exclusive down-regulation of a gene involved in cytokinin signaling, specifically TRITD-1Av1G198630 with a log2 fold of 5.74, which plays a role in cell division processes. Conversely, MRP3 treated with PSNPs displayed an overexpression of a gene associated with jasmonic acid signaling, TRITD_4Av1G002040, with a log2 fold of 3.98, which might be involved in plant-pathogen interaction mechanisms. Additional commonly enriched pathways included the Mitogen-activated protein kinases (MAPK) signaling pathway (ko04016), phosphonate and phosphinate metabolism (ko00440), starch and sucrose metabolism (ko00500), carotenoid (ko00906) biosynthesis, alpha-linolenic acid metabolism (ko00592), beta-alanine metabolism (ko00410) and ubiquinone and terpenoid-quinone biosynthesis (ko00130) (Fig. 5-A). Among the pathways exclusively enriched in PSNPs treated Kronos, valine, leucine, and isoleucine metabolism (ko00280), monoterpenoid biosynthesis (ko00902), fatty acid metabolism (ko00071), phagosome-related

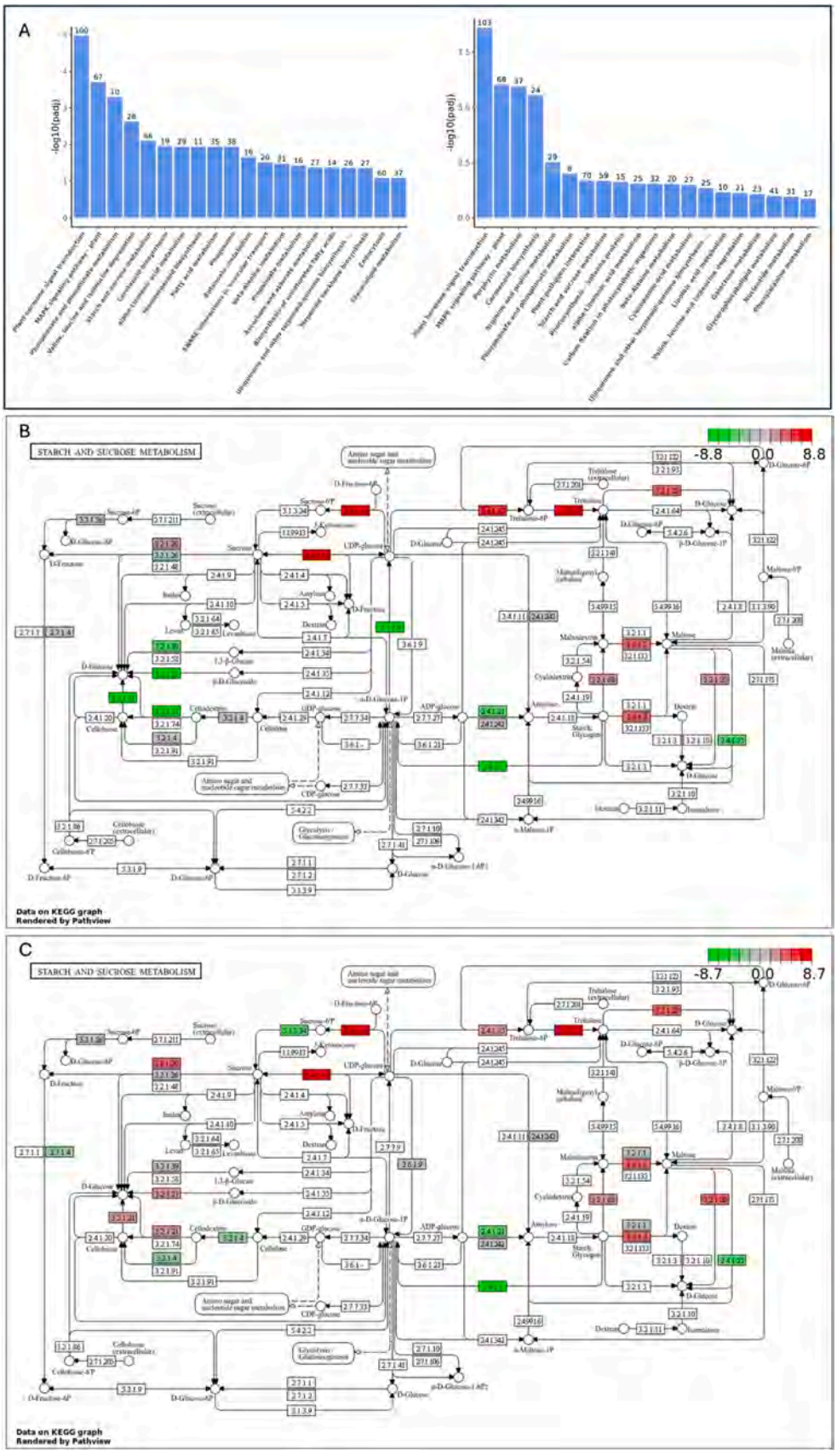

Fig. 6. KEGG enrichment analysis for Kronos_PSNPs and MRP3_PSNPs (A). Y axes correspond to the padj expressed as the base −10 logarithm of its values (-log10 (padj)). Higher values indicate greater significance. X axes correspond to the KEGG pathways. KEGG pathway's taes showing regulation of starch and sucrose of Kronos_PSNPs and MRP3_PSNPs (B).

processes (ko04145), butanoate metabolism, SNARE interactions in vesicular transport pathway (ko04130) and propanoate metabolism (ko00640), ascorbate and aldarate (ko00053), biosynthesis of unsaturated fatty acids (ko01040) and terpenoid backbone biosynthesis (ko00900), were revealed. The 6 significantly enriched pathways in MRP3 under PSNPs treatment were related to porphyrin and chlorophyll metabolism (ko00860), arginine and proline metabolism (ko00330), plant-pathogen interaction (ko04626), photosynthesis antenna proteins (ko00196), carbon fixation in photosynthetic organisms (ko00710), and cyanoamino acid metabolism (ko00460). For the photosynthetic pathway in MRP3 exposed to PSNPs, a visual representation of the structures of DEGs which contributed to the KEGG enrichment was reported from which emerged a downregulation of genes involved in the photosystem 2 efficiency, electron transport, oxygen evolving and light harvesting complexes (Fig. 6-A).

3.4.3.1. TAESoutput for significant genes related to starch and sucrose metabolic enzymes. Building upon the general KEGG pathway enrichment analysis, where starch and sucrose metabolism (ko00500) emerged as a significantly enriched pathway in both Kronos and MRP3 under PSNPs exposure, a detailed investigation into the specific enzymes regulated within this pathway was performed. This served to elucidate the transcriptional adjustments underlying carbohydrate allocation and energy management under PSNPs exposure. By mapping DEGs onto the KEGG starch and sucrose metabolism pathway, key enzymes involved in sucrose biosynthesis, sucrose catabolism, starch degradation, and trehalose metabolism, were identified, providing deeper insights into genotype-specific metabolic reprogramming (Fig. 6-A). Both Kronos and MRP3 exposed to the treatment showed upregulation of genes encoding sucrose phosphate synthase (EC 2.4.1.14). Kronos exhibited higher Log2FoldChange values for shared genes and uniquely displayed downregulated sucrose phosphate synthase-related genes (Table1 and Fig. 6-B). In contrast, MRP3 demonstrated a more uniform upregulation of sucrose phosphate synthase related genes, indicating a less dynamic response to PSNPs exposure (Table1 and Fig. 6-C). In both Kronos and MRP3 exposed to PSNPs genes for the sucrose synthase (EC 2.4.1.13) were significantly upregulated. Similarly, genes for beta-glucosidase (EC 3.2.1.20) and fructokinase (EC 2.7.1.4) were also upregulated in both wheat lines. Uniquely, the treated MRP3 displayed a strong downregulation of the UTP-glucose-1-phosphate uridylyl transferase (EC 2.7.7.9) gene (Table1) while uniquely in Kronos under PSNPs exposure, the alfa-amylase (EC 3.2.1.1) isoform responsible for active starch breakdown was upregulated(Table 1 and Fig. 6-A, B).Overall, these transcriptional changes suggest a genotype-specific reprogramming of carbon skeleton management in leaves under PSNP exposure, with Kronos preferentially mobilizing transitory starch to sustain energy-demanding stress responses, while MRP3 limits carbon flux toward UDP-glucose–dependent anabolic and cell wall–related pathways.

While some DEGs did not contribute to enriching the GO terms or KEGG pathways, their exceptionally high fold changes suggested a crucial role in the plant response to PSNPs treatment. Among these, aquaporin genes in Kronos treated with PSNPs stand out due to their involvement in water transport and cell elongation, respectively. Among these genes, two displayed particularly high fold changes the gene TRITD4Bv1G178880, with a Log2FoldChange of 3.48, that encodes aquaporin TIP1–1(https://www.uniprot.org/uniprotkb/O64964/entry)

Table 1
TAES for Sucrose and starch metabolism related genes significantly enriching the KEGG analysis of Kronos_PSNPs vs Kronos_Ctrl and MRP3_PSNPs vs MRP3_Ctrl with relative TAESnumber, EnsemblPlant accession number and Log2FoldChanges.

Enzyme	Genotype	TAES	GeneID	Log2FoldChange
Sucrose-phosphatesynthase (EC 2.4.1.14)	Kronos	taes:123063086	TRITD3Av1G243450	8.74
		taes:542872	TRITD3Av1G001690	2.64
		taes:123086738	TRITD4Av1G167490	-1.17
		taes:123071986	TRITD3Bv1G234800	3.47
		taes:123091244	TRITD4Bv1G032600	-1.40
	MRP3	taes:123063086	TRITD3Av1G243450	8.52
		taes:542872	TRITD3Av1G001690	1.76
		taes:542958	TRITD6Av1G051410	1.03
SucroseSynthase (EC 2.4.1.13)	Kronos	taes:123085854	TRITD4Av1G076300	4.12
		taes:123092190	TRITD4Bv1G104200	8.49
		taes:123129210	TRITD6Av1G226380	2.99
		taes:543390	TRITD7Bv1G024970	1.86
	MRP3	taes:123085854	TRITD4Av1G076300	4.00
		taes:123092190	TRITD4Bv1G104200	6.16
		taes:123129210	TRITD_6Av1G226380	2.00
		taes:543390	TRITD7Bv1G024970	2.00
Beta-glucosidase (EC 3.2.1.20)	Kronos	taes:101290655	TRITD4Bv1G197690	1.04
	MRP3	taes:123149090	TRITD7Av1G246990	2.33
UTP-glucose-1-phosphate uridylyltransferase (EC 2.7.7.9)	MRP3	taes:123143248	TRITD1Av1G148420	-7.20
Nucleoside-diphosphatase (EC 3.6.1.9)	Kronos	taes:123076153	TRITD3Av1G031550	-1.63
Fructokinase (EC 2.7.1.4)	Kronos	taes:123112568	TRITD5Bv1G159520	-2.19
	MRP3	taes:123062886	TRITD3Av1G233260	1.44
Alpha-amylase (EC 3.2.1.1)	Kronos	taes:123159470	TRITD7Bv1G160880	1.52
		taes:123061722	TRITD3Av1G166320	-1.03
Beta-amylase (EC 3.2.1.2)	Kronos	taes:123105923	TRITD5Av1G244830	5.82
		taes:123093753	TRITD4Bv1G193500	5.79
		taes:123090510	TRITD4Bv1G000620	-1.87
		taes:123188374	TRITD2Av1G084010	-3.09
		taes:123044617	TRITD2Bv1G089680	-2.28
	MRP3	taes:123105923	TRITD5Av1G244830	4.69
		taes:123093753	TRITD4Bv1G193500	4.51
		taes:123090510	TRITD4Bv1G000620	-1.77
		taes:123044617	TRITD2Bv1G089680	-1.40
		taes:123069423	TRITD3Bv1G074950	-1.14
Trehalase (EC 3.2.1.28)	Kronos	taes:123049002	TRITD1Av1G119750	2.34
		taes:123124209	TRITD1Bv1G117270	1.35
	MRP3	taes:123124209	TRITD1Bv1G117270	2.02
		taes:123049002	TRITD1Av1G119750	2.03

and the gene TRITD7Av1G176380, with a Log2FoldChange of 4.81, that encodes aquaporin TIP2–2. TIP1–1 and TIP2–2 (https://www.uniprot.org/uniprotkb/A0A9R0ZEY2/entry) are both members of the tonoplast intrinsic protein (TIP) family (Gattolinetal.,2011).

3.4.4. Gene set enrichment analysis (GSEA)

Building upon the significant enrichment of the starch and sucrose Metabolism pathway observed in the KEGG analysis, its downstream effects on energy metabolism were further investigated. Given the central role of glycolysis in carbohydrate breakdown and ATP production, it was performed a GSEA to assess the transcriptional regulation of the Glycolysis/Gluconeogenesis pathway (TAES00010) as cascade effects of 50 nm PSNPs exposure. The GSEA enrichment plot for the Glycolysis/Gluconeogenesis (TAES00010) pathway in Kronos exposed to PSNPs, showed a positive enrichment score (ES), indicating that genes associated with this pathway are predominantly upregulated in Kronos under PSNPs exposure (Fig. 7-B). The enrichment profile reaches its ES peak in the early ranks of the ordered gene list, suggesting that glycolysis-related genes are among the most strongly upregulated in the dataset. The black vertical bars represent the position of pathway-related genes in the ranked list, showing a concentration towards the left side of the plot, further supporting a significant positive enrichment. The point of zero enrichment score crossing is observed at around rank 20,642, indicating the threshold at which the pathway no longer shows positive enrichment The ranking metric plot (bottom panel) illustrates the signal-to-noise ratio of individual genes, with a clear shift favoring genes enriched in Kronos exposed to PSNPs (left side) compared to the control (Fig. 7-B). The analysis did not show any enrichment for the glycolysis/gluconeogenesis (TAES00010) pathway in MRP3.

3.5. Carbohydrate and proline content

Following transcriptomic outputs, starch, alpha-amylase's activity and sugar measurements were performed to confirm the results obtained regarding the gene expression regulation induced by 50 nm PSNPs exposure. Specifically, the total starch was measured as well as sucrose, glucose, and fructose. The total starch content significantly decreased in Kronos exposed to PSNPs while it was not affected by PSNPs treatments in MRP3 (Fig. 8-A). The alpha-amylase's activity was higher only in Kronos treated with PSNPs with no variations in MRP3 (Fig. 8-B). PSNPs notably increased sucrose levels in Kronos while it was decreased in MRP3 by PSNPs exposure (Fig. 8-C). Glucose content was significantly increased in Kronos in response to PSNPs compared to control conditions. Similarly, MRP3 showed a significant increase in glucose when exposed to PSNPs (Fig. 8-D). PSNPs exposure caused an increase in fructose content in both Kronos and MRP3 (Fig. 8-E). Measuring proline, an osmolyte, key molecule that acts as regulator for water depletion induced mechanisms in plants, was useful to address a potential induction of osmotic stress response in Kronos and/or MRP3. Proline content resembled control like levels in Kronos treated with PSNPs while increased in MRP3 treated samples (Fig. 8-F)

4. Discussion

As for many other xenobiotics present in soil, plants can absorb PSNPs, potentially altering their physiology and metabolism. Although numerous studies have investigated the metabolic imbalances induced by various xenobiotics, the effects of PSNPs on crop physiology remain largely underexplored. The comparison between the effects of PSNPs exposure on the wild type Kronos and MRP3, a mutant with the same genetic background, impaired in the multidrug resistance-associated protein 3 (also functioning as a phytic acid transporter (Frittellietal., 2023), provides new insights into the potential pathways involved in PSNPs sensing and detoxification. In animals, MRP3 is known as a transporter of endotoxins and xenobiotics, contributing, alongside other MRP-related proteins, to resistance against natural and synthetic drugs and their conjugated metabolites (Ghanem and Manautou, 2019). In plants, MRPs have also been reported to sequester xenobiotics into vacuoles, thereby maintaining cellular homeostasis. For instance, they contribute to herbicide resistance in Arabidopsis (Leslie et al., 2001).

4.1. Uptake and aggregation of PSNPs in durum wheat

While soil-based systems are essential to capture the complexity of

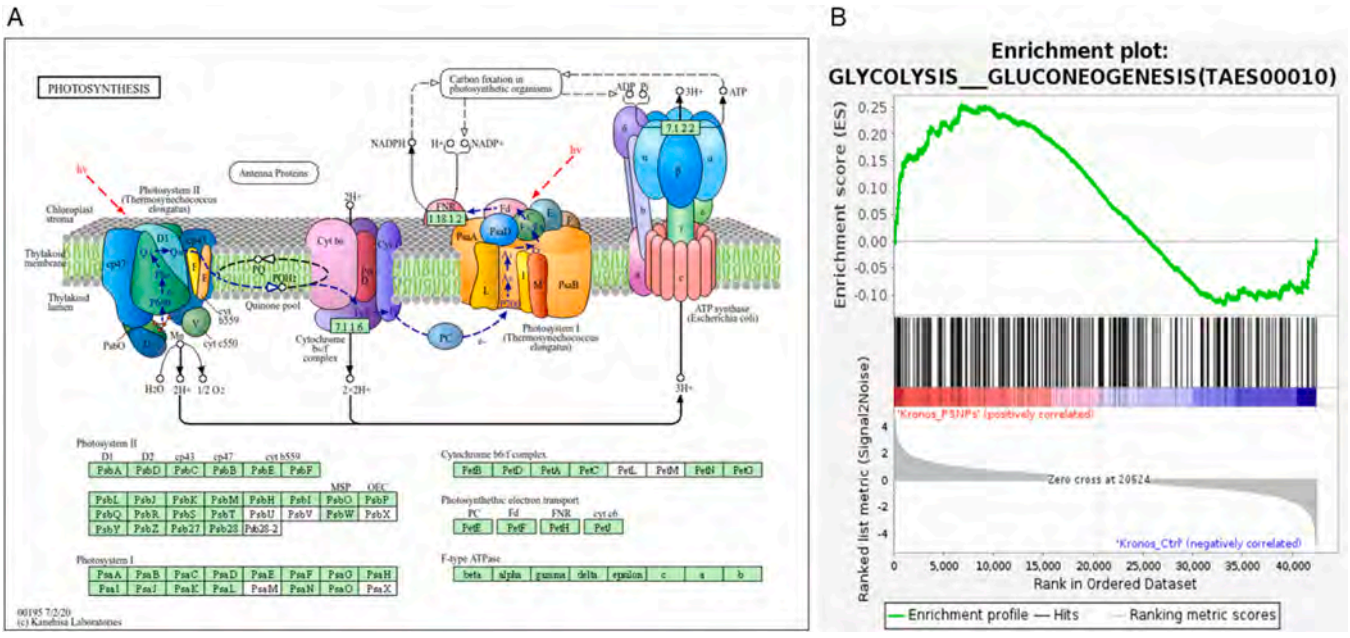

Fig. 7. Visual representation of the photosynthetic compartments of which genes were enriched in the KEGG analysis for MRP3_PSNPs (A). Plot showing the enrichment profile (green curve) of the Glycolysis/Gluconeogenesis pathway, indicating a positive enrichment score (ES) in Kronos_PSNPs (B). The black vertical bars represent the positions of pathway-related genes in the ranked dataset, showing a concentration towards the left, which suggested their upregulation in Kronos_PSNPs.

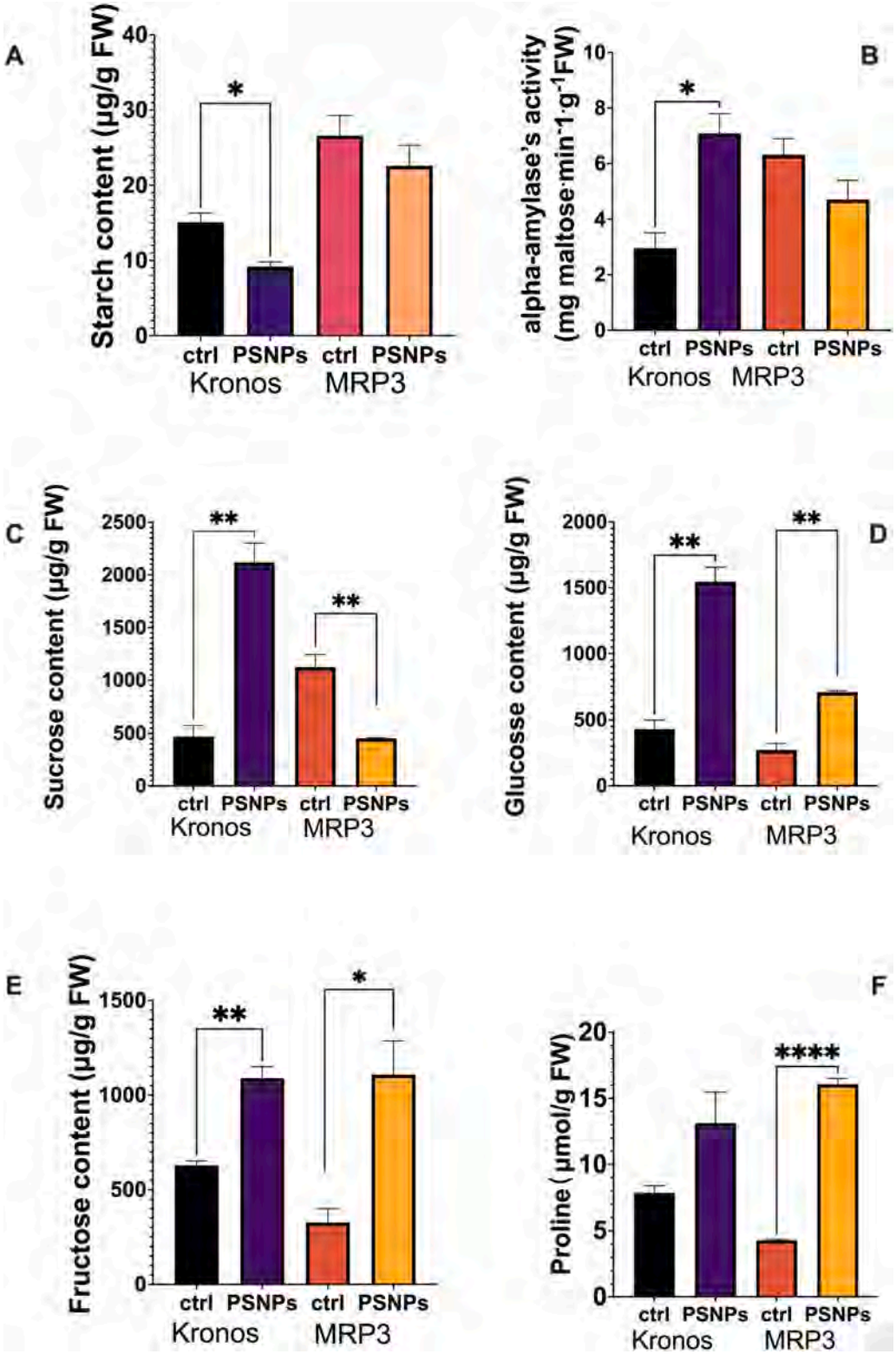

Fig. 8. Effects of 50 nm PSNPs and 100 nm PSNPs on the starch content (A), expressed as µg/g FW and alpha-amylase's activity (B), expressed as mg maltose min^{-1} g^{-1}; Effect of 50 nm PSNPs on sucrose (C), glucose (D) and fructose content (E), described as µg/g FW. Effects of 50 nm PSNPs on the proline content expressed as µmol/g FW (F). Data are presented as mean ± SEM (n = 3); Tukey's $p < 0.05$. Significant differences among pairwise comparisons are represented with asterisks (* $p < 0.05$; ** $p < 0.01$; *** $p < 0.001$; **** $p < 0.0001$).

field conditions, including interactions with soil physicochemical and biological components, the hydroponic approach adopted here was intentionally chosen to minimize environmental variability and to specifically dissect genotype-dependent plant responses to nanoplastic exposure. The data here presented demonstrated that PSNPs penetrate durum wheat roots in both Kronos and MRP3 plants. Their presence as aggregates of nanoparticles is well evident in different tissues of the roots. This aligns with previous research indicating that plastic

nanoparticles can enter root tips through the rhizodermis via intercellwall pathways, even if the mechanisms by which PSNPs traverse the cortex or cross the Casparian strip to reach the xylem remain unclear (Lianetal.,2020). Similarly, Xiao et al. (2022) reported PSNPs accumulation in duckweed roots and fronds under environmentally relevant concentrations, while another study observed PSNPs in Arabidopsis roots, including root hairs, intracellular spaces, stele and xylem (Sunetal.,2020;Xiaoetal.,2022). Our results indicate that in wheat, PSNPs were also translocated to root xylem, as it is suggested by their presence in the vascular system of the leaves, in agreement with a root to shoot translocation.

4.2. Genotype-dependent physiological responses to PSNPs exposure

According to the phenotyping characterization and most of the biochemical parameters analyzed in Kronos and MRP3 exposed to PSNPs, minor differences are evident between the alterations induced by PSNPs of 50 and 100 nm (Fig. 1 and Fig. 3), thus suggesting that the different nominal size of the nanoparticles in this range has relatively low relevance in affecting plants responses.

It is important to note that confocal microscopy does not allow direct visualization of individual PSNPs due to their size being below the optical resolution limit. Consequently, the micrometer-scale fluorescent structures observed in root tissues are most likely attributable to localized fluorescence accumulations or potential PSNPs aggregates rather than single particles. Aggregates of excessive size are not expected to be translocated and are likely retained at the root level.

Any potential movement of PSNP-associated signal is therefore discussed in relation to particle fractions that may fall within the nanometer size range reported in the literature to be compatible with xylem transport. Accordingly, interpretations regarding PSNPs internalization and transport are qualitative and hypothesis-driven rather than quantitative or mechanistically resolved. Therefore, it was not possible to establish whether the amount of PSNPs taken up by the two genotypes were different. However, it is interesting to note that the phenotyping characterization of Kronos and MRP3 plants exposed to PSNPs clearly shows different effects. PSNPs exposure did not have any negative effects on Kronos plants, at least in the stage of development here studied. Rather on the contrary, in Kronos, PSNPs exposure induced an increase in roots and shoot length as well as in plant biomass and number of leaves. On the other hand, in MRP3, PSNPs induced a decrease in plant biomass and oxidative stress supported by a significant increase in MDA accumulation (Figs. 1-D and 3-H). This evidence suggested that the alteration in the ability to translocate xenobiotics into the vacuole, caused by the mutation induced in the MRP3 wheat, might play a significant role in protecting the plant from the effects of PSNPs. However, it is known that the suppression in a specific cellular activity often leads to several pleiotropic alterations that could also be responsible for the different sensitivity to PSNPs observed in the mutant. Future high-resolution or correlative imaging approaches will be required to precisely determine PSNPs size, aggregation state, and intracellular versus apoplastic localization within plant tissues.

4.3. Transcriptomic and metabolic reprogramming induced by PSNPs

PSNPs caused physiological and metabolic alterations in the plants as possible cascade effects of PSNPs – dependent alteration in gene expression, as confirmed by the transcriptomic analyses. The decision to restrict transcriptomic analyses to the 50 nm PSNP treatment was based on the observation that this condition elicited a coordinated and genotype-dependent physiological and metabolic response, whereas exposure to 100 nm PSNPs predominantly induced more generalized stress-related effects, potentially involving distinct and rapidly activated response pathways. Indeed, such alteration was only in part common to the two genotypes. Indeed, both Kronos and MRP3 showed GO enrichment in the acid chemical, abiotic stimulus, and water response after PSNPs exposure. Consistently, in Arabidopsis plants exposed to PSNPs the main upregulated GO terms were like those upregulated by abiotic factors and water depletion (Sunetal.,2020) and in duckweed the PSNPs exposure increased the expression of genes related to the response of osmotic stress (Xiaoetal.,2022). Interestingly, all DEGs related to acid chemicals, abiotic stimulus, and water response evidenced by GO analyses were related to the metabolism of dehydrins, molecules that regulate osmotic stress responses in plants (CloseandLammers,1993). This highlighted a common stress response mechanism possibly induced by PSNPs exposure in both Kronos and MRP3. However, the KEGG analysis highlighted that the two genotypes responded in different ways to osmotic stress. For instance, MRP3 displayed a PSNPs-dependent upregulation of the genes involved in the biosynthesis of proline (Fig. 6-A), a well-known osmolyte involved in responses against osmotic stress (Yanetal.,2025). Such upregulation was confirmed by the increased levels of proline content in MRP3 exposed to PSNPs (Fig. 8-F). On the other hand, exclusively in Kronos the exposure to PSNPs induces a particularly high fold changes in two aquaporin genes: TIP1–1 and TIP2–2, both members of the tonoplast intrinsic protein (TIP) family. TIP1–1 is a water channel that promotes rapid water influx during cell expansion, contributing to osmotic equilibration and transcellular water flow (Chaumontetal.,1998). TIP2–2 works as a tonoplastic channel for water and small neutral molecules and is crucial for maintaining osmotic balance and regulating cell turgor (Uenishietal.,2014). The upregulation of these genes could help Kronos to better guarantee water homeostasis compared to MRP3, at the onset of the osmotic stress induced by PSNPs. This was also suggested by the absence of a proline increase in Kronos exposed to PSNPs. The presence of an osmotic stress was supported by the reduced transpiration and gas exchange occurred after exposure to PSNPs in both genotypes (Fig. 3- C, D). The water response induced by PSNPs exposure hypothetically occurs because PSNPs tend to form aggregates, as demonstrated by the fact that the size of fluorescent dots visible both in roots and in leaves have a much higher dimension than those used for the treatments(Khanetal.,2024).We therefore speculate that an eventual generation of PSNPs aggregates within plants, might block pores for water transport, thus inducing a response that resembles water deprivation or drought. Moreover, the response to abiotic stimulus, emerged from GO, suggested that plants perceived PSNPs as xenobiotic and activate responses that are characteristic of abiotic stress (Dzierżyńskietal.,2024;Sobraletal.,2025; Suleiman,U.F.andIbrahim, S., 2024; Vicidominietal.,2024).

Another interesting effect of PSNPs exposure was the alteration of sugar metabolism that occurred in both genotypes, again with some differences. In both genotypes, a PSNPs-dependent increase in glucose accumulation was registered, while a decrease in starch was statistically significant only in Kronos (Fig. 8-A). This suggested that particularly in Kronos, a metabolic shift occurred from carbohydrates storage to immediate energy mobilization, likely as an adaptive response to osmotic stress (Darkoetal.,2019). The presence of PSNPs induced an opposite effect also in sucrose levels that increased in Kronos and decreased in MRP3. Moreover, glucose and fructose act as osmolytes and their role in sensing stress condition is well known (Lietal.,2021). Coherently, GO analysis highlighted the enrichment of carbohydrate metabolic processes, particularly in Kronos.Indeed, an enzyme-resolved inspection of the sucrose pathway, based on EC annotations emerging from KEGG and TAES, confirmed that PSNPs exposure induced expression regulation of several genes encoding sucrose-related metabolism, targeting multiple enzymatic nodes rather than a single step (Fig. 6-B, C). In particular, genes encoding sucrose-phosphate synthase (EC 2.4.1.14), sucrose synthase (EC 2.4.1.13), and invertase-related enzymes (EC 3.2.1.26) were modulated in both genotypes (Table1 and Fig. 6-B, C). However, Kronos exhibited slightly higher Log2FoldChange values for the same genes upregulated in MRP3 and uniquely displayed downregulated sucrose phosphate synthase-related genes, enzyme responsible for sucrose catabolism (Table1 and Fig. 6-B). Moreover, Kronos displayed the enrichment of alpha-glucosidase and glycolysis-linked EC classes, while

MRP3 showed repression of UTP-glucose-1-phosphate uridylyl transferase (EC 2.4.1.13), a pivotal enzyme for UDP-glucose supply to sucrose biosynthesis (Table1 and Fig. 6-C). The UDP-glucose pool represents a central hub controlling the balance between synthesis, catabolism, and cell-wall associated sinks. The downregulation of this EC in MRP3 may suggest a constriction limiting the transcriptional compensation of sucrose flux, consistently with the decreased level of sucrose and with the mutant's reduced growth. Therefore, our interpretation does not intend to claim a directly proven enzymatic balance, but rather that EC-annotated transcriptomic coverage provides a coherent framework to infer a more flexible carbon allocation in Kronos than in MRP3 under PSNPs exposure. Complexly, MRP3 demonstrated a more uniform upregulation of sucrose phosphate synthase related genes, indicating a less dynamic response to PSNPs exposure (Table 1 and Fig. 6-C). In particular, the downregulation of the gene for UTP-glucose-1-phosphate uridylyl transferase in MRP3, being a critical enzyme for UDP-glucose biosynthesis, may indicate a bottleneck in the sucrose biosynthetic pathway, limiting its production in the mutantas reflected by the reduced sucrose levels quantified in MRP3 (Fig. 6-B and Table1).While sucrose-related enzymatic activities were not directly measured, the combined metabolic profile and transcriptomic analyses provide a coherent framework to interpret genotype-dependent differences in sucrose dynamics under PSNPs exposure, suggesting a genotype-specific regulation of sucrose metabolism in Kronos. This genotype exhibited increased alpha-amylase's activity and gene expression, supported by the reduced starch level under PSNPs exposure (Fig. 8-A, B). It is interesting that literature evidence shows that PSNPs may act as "nanocatalysts" for alpha-amylase activity, thus enhancing its activity (Lianetal.,2020). PSNPs were also reported to interact *in vitro* with alpha-amylase altering its secondary structure (Azhagesanetal.,2022). The GSEA analysis further revealed a positive enrichment score for glycolysis-related genes in Kronos, absent in MRP3. This further supported a higher efficiency of Kronos to shift its carbohydrate metabolism towards an increased glycolytic flux to maintain ATP production that could be pivotal for better counteracting the stress impairment. This was consistent with the data of Zhang and co-workers (2022), who proposed that PSNPs exposure changed *Zea mais* basal energy metabolism and those of Zhou and co-workers (2021) showing an increase in soluble sugars and a decrease in starch in rice roots (Zhang et al., 2022; Zhou et al., 2021).

In their whole, the alteration in carbohydrates levels and related gene-expression induced by PSNPs in the two genotypes underlined the relevance of this metabolism in overcoming the negative effects of PSNPs. The shift toward an increased carbohydrate metabolism in Kronos could be relevant not only for overcoming the effects of PSNPs-dependent stresses but also for sustaining growth, therefore explaining the observed increase induced by PSNPs exposure in this genotype. Notably, having Kronos a more coordinated transcriptional reprogramming than MRP3 (Table 1), might be a determinant for the phenotypic outcome of PSNPs exposure, rather than isolated gene effects.

Another metabolic pathway altered by PSNPs is that related to carotenoids biosynthesis. Carotenoids play a crucial role in providing plants with a tolerance to a series of abiotic stresses, comprising PSNPs (Uarrotaetal.,2018). Even if in both genotypes exposed to 50 nm PSNPs, genes related to these biosynthetic pathways were up-regulated, only in Kronos a significant increase in carotenoid level occurred in leaves after PSNPs exposure. On the other hand, no difference was evident in the MRP3 plants exposed to 50 nm PSNPs and a significant decrease occurred after exposure to 100 nm PSNPs (Fig. 3-G). This evidence also suggested a higher capacity of Kronos to activate antioxidant/protective mechanisms against PSNPs exposure in comparison with MRP3.

PSNPs exposure differently affected the two genotypes in several other parameters related to photosynthesis. A key difference between the two genotypes was that transcriptional repression of the photosynthesis occurred only in MRP3 (Figs. 6-A and 7-A). These transcriptomic results were consistent with the reduced PhiPS2 and ETR observed in MRP3 PSNPs exposed plants compared to controls (Fig. 3-A and B). On the contrary, Kronos, which did not show expression alterations in photosynthesis-related genes, displayed an increase in PhiPS2 and ETR in response to PSNPs treatments and showed an increase in chlorophyll. However, Kronos showed a decreased gsw exchange and transpiration rate as well as MRP3, suggesting an early marker of stress that cannot be sustainable in the long-term exposure scenario. It is important to remark that photosynthetic performance under stress conditions is not exclusively driven by stomatal regulation, and genotype-specific acclimation could result in a partial decoupling between gas exchange parameters and photosynthetic efficiency. The main reason for this, is attributable to the fact that gsw, which represents the stomatal conductance, and the transpiration rate, are mainly controlled by CO2 entrance, while PhiPS2 and ETR reflect the photochemical activity, associated with active sink metabolites as sugars, active growth and an efficient photoprotection, given by carotenoids and other pigments (Flexas and Medrano, 2002; Baker, 2008; Murchie and Lawson, 2013; Flexas et al., 2004). These observations and overall results as the observed increase in sugars related metabolism genes (Table 1 and Fig. 6-B), sugars content (Fig. 8-C, D, E) and carotenoids content (Fig. 3-G), are coherent with the ability of Kronos to preserve photosynthesis efficiently under PSNPs stress following 21 days of exposure. This response is consistent with its enhanced capacity to sustain plant growth. Conversely, in MRP3the impairment of photosynthetic performance evidenced by reduced transcription for photosynthetic genes (Fig. 7) and reduced photosynthetic parameters (Fig. 3-A, B) is reflected in the reduced levels of sucrose and biomass accumulation (Figs. 8-C and 1-D). An increase in photosynthesis and chlorophyll content was shown in bread wheat (Lian et al., 2020). However, other literature data indicate a negative effect of PSNPs exposure on photosynthesis and chlorophyll contents. For example, *Haematococcus pluvialis* exposed to varying PSNPs concentrations, revealed a dose-dependent reduction in photosynthesis (YingyingZhangetal.,2024) and a decrease in photosynthetic parameters has also been reported in red lettuce exposed to PSNPs (Dongetal.,2021). These different behaviours could be due to the species – specific capacity to respond to the stress, but even to the different conditions of PSNPs exposure (duration of exposure, nanoparticles concentration, stage of development of the plants) and mostly, to the genotype-specific traits.

4.4. Role of TdMRP3 in genotype-specific sensitivity to PSNPs

Overall findings, suggested that MRP3 mutant was more susceptible to PSNPs exposure than Kronos, aligned by MRP3's reduced growth, impaired photosynthetic capacity, increased proline and MDA content, and failure to maintain a balance within energy storage metabolism and energy mobilization, in response to the treatments. Apart the possible impairment in translocating xenobiotics into vacuoles, the capacity of MRP3 to act as phytic acid transporter could also have an impact on the behaviour of the MPR3 genotype exposed to PSNPs. Hypothetically, the alteration in phytic acid transport and distribution could influence the cation transport within MRP3 plants, since it typically forms complexes with cations, reducing the concentration of their free forms. Therefore, the impaired phytic acid distribution may change cations uptake and/or the distribution/accumulation of their free forms as it has been proven to occur in MRP3 seeds (Frittellietal.,2023). Since PSNPs commonly form complexes with cations, it is reasonable to speculate that PSNPs transport and accumulation may also be promoted more in MRP3 than in Kronos. A hypothetic increased transport and accumulation of PSNPs may induce a reduced capability to adopt an efficient adaptive stress response in MRP3, leading to a more evident PSNPs-induced toxicological damage. This genotype-specific diverse MRP3 response in carbohydrates metabolism, coupled with MRP3 reduced growth and photosynthetic impairment, indicated that the enhanced transcriptional activation of sucrose synthase genes is insufficient to compensate for the increased energy demand, resulting in preferential energy mobilization alone, rather than storage. These findings suggested that MRP3 struggles

to compensate for PSNPs induced carbohydrate imbalances, whereas Kronos adopts a more flexible and efficient metabolic strategy. Importantly, rather than being solely attributable to a more pronounced osmotic stress in MRP3, these responses reflect genotype-specific differences in carbon allocation, energy demand, and stress acclimation strategies under PSNPs exposure, likely due to its mutation, implying a possible role of the *TdMRP3* gene in PSNPs resilience. However, this remains speculative and requires direct evidence.

5. Conclusion

This study provides novel insights into the physiological, metabolic, and transcriptomic responses of durum wheat exposed to short-term (21 days) PSNPs in the stage of young plants (5 days after germination) highlighting the relevance of genotype-specific traits in modulating plant tolerance to emerging pollutants. Our data demonstrate that PSNPs were internalized and translocated in both wild-type Kronos and its MRP3 mutant derivative, although the two genotypes exhibit strikingly divergent responses (Fig. 9).While Kronos appears to activate effective metabolic and molecular mechanisms to compensate for PSNP-induced stress, reflected by enhanced growth, photosynthetic performance, and activation of osmotic adjustment pathways, MRP3 shows clear signs of physiological impairment, including reduced biomass, increased lipid peroxidation and proline accumulation, and a generalized repression of photosynthesis-related genes. Kronos activates an adaptive response involving dehydrins and aquaporin, maintaining a balance between sucrose synthesis and breakdown and probably ensuring energy homeostasis. Conversely, MRP3 increases proline accumulation and, instead of sustaining sucrose synthesis, predominantly undergoes sucrose catabolism, favoring an immediate energy mobilization strategy that does not sustain growth. Additionally, MRP3 exhibits progressive photosynthetic impairment, further reducing its ability to adapt and signs of oxidative stress. The stimulatory effects of PSNPs on plant growth observed in Kronos were surprising even if it is coherent with the increase in photosynthetic efficiency and energy metabolism. However, it must be underlined that these metabolic changes observed in Kronos could be an adaptive response to PSNP-induced stress, helping to maintain energy balance only in the short term. In the long-term exposure to PSNPs, a prolonged reduction in Gsw and transpiration rate coupled with the simple sugars increase is not sustainable and could have negative consequences even in Kronos, particularly for yield. Moreover, an excessive accumulation of sugars was linked to premature senescence (Lietal.,2019). Therefore, over time, PSNPs may induce negative effects in both genotypes, with MRP3 being still more susceptible. Further research is needed to assess the long-term consequences of chronic PSNPs as well as if the PSNPs route ends in the leaves or can reach flowers and seeds. Future studies integrating detailed physiochemical characterization of PSNPs in hydroponic solutions, aged NPs, additional polymer types, and soil-based systems will be essential to further extend the ecological relevance of the findings presented here. Particularly, although size-dependent effects are discussed with reference to the nominal properties of the PSNPs provided by the manufacturer prior to hydroponic contamination, without the study of their behaviour in Hogland's solutions, we cannot exclude that dynamic processes such as aggregation or surface modification may occur in the hydroponic medium and contribute to the observed responses. It will also be relevant to better identify the intra and inter-cellular route of PSNPs during their journey from roots to aerial parts of the plants and to quantify the actual PSNPs uptake, to provide direct evidence of MRP3 vacuolar sequestration hypothetically being impaired in the mutant.

CRediT authorship contribution statement

Francesco Sestili: Writing – review & editing, Supervision, Resources, Investigation, Funding acquisition, Conceptualization. **Vittoria Locato:** Writing – review & editing, Supervision, Investigation. **Laura De Gara:** Writing – review & editing, Visualization, Supervision, Resources, Funding acquisition, Conceptualization. **Sara Cimini:** Writing – review & editing, Writing – original draft, Validation, Supervision, Methodology, Data curation, Conceptualization. **Benedetta Pizziconi:** Writing – review & editing, Writing – original draft, Validation, Methodology, Formal analysis, Data curation, Conceptualization. **Samuela Palombieri:** Writing – review & editing, Supervision, Methodology, Formal analysis, Conceptualization. **Giuliana Bruno:** Writing – review

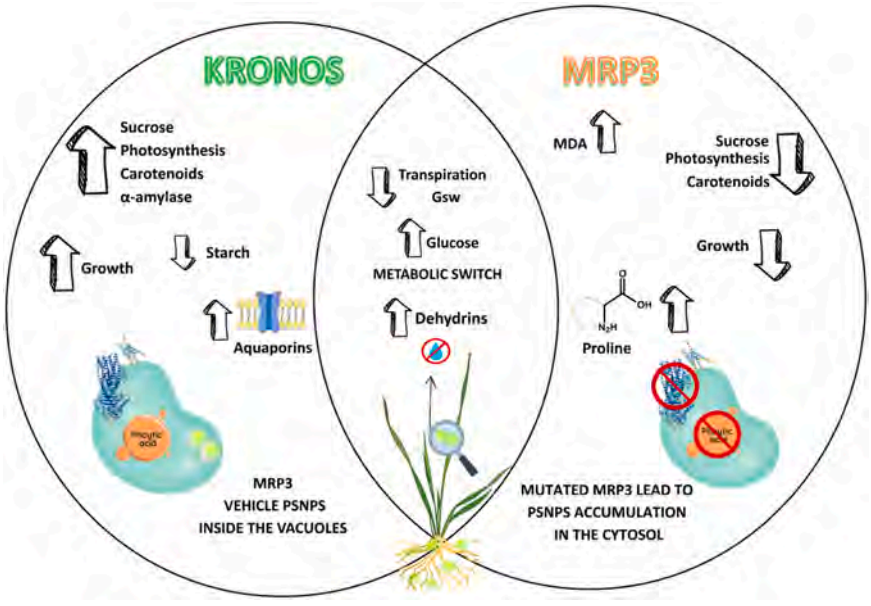

Fig. 9. Schematic representation of the contrasting responses of Kronos and the MRP3 mutant to PSNPs. In Kronos (left panel), PSNPs were sequestered inside the vacuoles via the MRP3 transporter, allowing the plant to sustain growth, photosynthesis, carotenoid accumulation, sucrose metabolism, and alpha-amylase's activity, while reducing starch levels. Enhanced aquaporin expression supported water balance. In the MRP3 mutant (right panel), the loss of the MRP3 function prevents proper vacuolar sequestration, leading to PSNPs accumulation in the cytosol. This condition was associated with decreased photosynthesis, carotenoids, and growth, together with enhanced proline accumulation, higher MDA content, reduced transpiration and stomatal conductance, and a metabolic switch towards stress-protective mechanisms, including dehydrin induction.

& editing, Validation, Methodology, Formal analysis, Data curation.

Funding

This study was funded by the European Union Next-Generation EU (PIANO NAZIONALE DI RIPRESA E RESILIENZA (PNRR) – MISSIONE 4 COMPONENTE 2, INVESTIMENTO 1.4 – D.D. 1032 17/06/2022), grant number: CN00000022 - National Research Centre for Agricultural Technologies (Agritech) and by the Ministry for Education, University, and Research (MIUR) initiative "Department of Excellence" (Law 232/2016) DAFNE Project 2023–27 "Digital, Intelligent, Green and Sustainable (acronym: D.I.Ver.So)".

Declaration of Competing Interest

The authors declare that they have no conflict of interest or any financial and personal relationships with other people or organizations that could inappropriately influence their work.

Appendix A. Supporting information

Supplementary data associated with this article can be found in the online version at doi:10.1016/j.plana.2026.100274.

Data availability

Data will be made available on request.

References

Adamczyk, S., Chojak-Koźniewska, J., Oleszczuk, S., Michalski, K., Velmala, S., Zantis, L. J., Bosker, T., Zimny, J., Adamczyk, B., Sowa, S., 2023. Polystyrenenanoparticles induce concertedresponse of plant defense mechanisms in plantcells. Sci. Rep. 13, 22423. https://doi.org/10.1038/s41598-023-50104-5.

Azhagesan, A., Chandrasekaran, N., Mukherjee, A., 2022. Multispectroscopyanalysis of polystyrenenanoplastic interaction with diastase α-amylase. Ecotoxicol. Environ. 247, 114226. https://doi.org/10.1016/j.ecoenv.2022.114226.

Baker, N.R., 2008. Chlorophyll fluorescence: a probe of photosynthesis in vivo. Annu. Rev. Plant Biol. 59, 89–113. https://doi.org/10.1146/annurev.arplant.59.032607.092759.

Carillo, P., Gibon, Y., 2011. PROTOCOL: Extraction and determination of proline. PrometheusWiki.

Chaumont, F., Barrieu, F., Herman, E.M., Chrispeels, M.J., 1998. Characterization of a maizetonoplastaquaporinexpressed in zones of celldivision and elongation. Plant Physiol. 117, 1143–1152. https://doi.org/10.1104/pp.117.4.1143.

Cimini, S., Locato, V., Giacinti, V., Molinari, M., De Gara, L., 2022. A multifactorial regulation of glutathione metabolism behind salt tolerance in rice. Antioxidants 11 (6), 1114. https://doi.org/10.3390/antiox11061114.

Ciudad-Mulero, M., Barros, L., Fernandes, Â., Ferreira, I.C.F.R., Callejo, M.J., Matallana-González, M.C., Fernández-Ruiz, V., Morales, P., Carrillo, J.M., 2020. Potential health claims of durum and bread wheatfloursasfunctionalingredients. Nutrients 12, 204. https://doi.org/10.3390/nu12020504.

Close, T.J., Lammers, P.J., 1993. An osmotic stress protein of cyanobacteriaisimmunologicallyrelated to plantdehydrins. Plant Physiol. 101, 773–779. https://doi.org/10.1104/pp.101.3.773.

Cole, L., Fernandes, D., Hussain, M.T., Kaszuba, M., Stenson, J., Markova, N., 2021. Characterization of Recombinant Adeno-Associated Viruses (rAAVs) for Gene Therapy Using Orthogonal Techniques. Plant Nanobiology 13 (4), 586. https://doi.org/10.3390/pharmaceutics13040586.

Condò, I., Pizziconi, B., Cimini, S., Trombetta, M., De Gara, L., Schena, E., Giannitelli, S. M., Lo Presti, D., 2025. An innovative self-adhesive wearable sensorbased on fiber Bragg gratingtechnology for plantgrowth monitoring. IEEE Sens. J. 25 (2), 2705–2713. https://doi.org/10.1109/JSEN.2024.3502486.

Darko, E., Végh, B., Khalil, R., Marček, T., Szalai, G., Pál, M., Janda, T., 2019. Metabolicresponses of wheat seedlings to osmotic stress induced by variousosmolytes under iso-osmoticconditions. PLoS ONE 14, e0226151. https://doi.org/10.1371/journal.pone.0226151.

Dong, Y., Song, Z., Liu, Y., Gao, M., 2021. Polystyreneparticlescombined with di-butylphthalate cause significantdecrease in photosynthesis and red lettucequality. Environ. Pollut. 278, 116871. https://doi.org/10.1016/j.envpol.2021.116871.

Dzierżyński, E., Gawlik, P.J., Puźniak, D., Flieger, W., Jóźwik, K., Teresiński, G., Forma, A., Wdowiak, P., Baj, J., Flieger, J., 2024. Microplastics in the human body: exposure, detection, and risk of carcinogenesis: a state-of-the-art review. Cancers 16, 3703. https://doi.org/10.3390/cancers16213703.

Flexas, J., Bota, J., Loreto, F., Cornic, G., Sharkey, T.D., 2004. Diffusive and metabolic limitations to photosynthesis under drought and salinity in C3 plants. Plant Biol. 6, 269–279. https://doi.org/10.1055/s-2004-82086.

Flexas, J., Medrano, H., 2002. Drought inhibition of photosynthesis in C3 plants: stomatal and non-stomatal limitations revisited. Ann. Bot. 89, 183–189. https://doi.org/10.1093/aob/mcf027.

Frittelli, A., Botticella, E., Palombieri, S., Masci, S., Celletti, S., Fontanella, M.C., Astolfi, S., De Vita, P., Volpato, M., Sestili, F., 2023. The suppression of TdMRP3 genesreduces the phytic acid and increases the nutrientaccumulation in durumwheatgrain. Front. Plant Sci. 14, 1079559. https://doi.org/10.3389/fpls.2023.1079559.

Gattolin, S., Sorieul, M., Frigerio, L., 2011. Mapping of tonoplastintrinsicproteins in maturing and germinatingArabidopsisseedsreveals dual localization of embryonicTIPs to the tonoplast and plasma membrane. Mol. Plant 4, 180–189. https://doi.org/10.1093/mp/ssq051.

Ghanem, C.I., Manautou, J.E., 2019. Modulation of hepatic MRP3/ABCC3 by xenobiotics and pathophysiological conditions: Role in drug pharmacokinetics. Curr. Med. Chem. 26, 1185–1223. https://doi.org/10.2174/0929867325666180221142315.

Gong, W., Zhang, W., Jiang, M., Li, S., Liang, G., Bu, Q., Xu, L., Zhu, H., Lu, A., 2021. Species-dependentresponse of food crops to polystyrenenanoplastics and microplastics. Sci. Total Environ. 796, 148750. https://doi.org/10.1016/j.scitotenv.2021.148750.

Grosse-Heilmann, M., Cristiano, E., Deidda, R., Viola, F., 2024. Durumwheatproductivitytoday and tomorrow: a review of influencingfactors and climatechangeeffects. Resour. Environ. Sustain. 17, 100170. https://doi.org/10.1016/j.resenv.2024.100170.

Khan, A.R., Ulhassan, Z., Li, G., Lou, J., Iqbal, B., Salam, A., Azhar, W., Batool, S., Zhao, T., Li, K., Zhang, Q., Zhao, X., Du, D., 2024. Micro/nanoplastics: critical review of their impacts on plants, interactions with othercontaminants (antibiotics, heavy metals, and polycyclicaromatichydrocarbons), and management strategies. Sci. Total Environ. 912, 169420. https://doi.org/10.1016/j.scitotenv.2023.169420.

Kik, K., Bukowska, B., Sicińska, P., 2020. Polystyrenenanoparticles: sources, occurrence in the environment, distribution in tissues, accumulation and toxicity to variousorganisms. Environ. Pollut. 262, 114297. https://doi.org/10.1016/j.envpol.2020.114297.

Kim, S.W., Kim, D., Chae, Y., Kim, D., An, Y.-J., 2019. Crop-dependentchanges in water absorption of expandedpolystyrene in soilenvironments. Chemosphere 219, 345–350. https://doi.org/10.1016/j.chemosphere.2018.12.057.

Leslie, E.M., Ito, K., Upadhyaya, P., Hecht, S.S., Deeley, R.G., Cole, S.P.C., 2001. Transport of the β-O-glucuronide conjugate of the tobacco-specific carcinogen 4-(methylnitrosamino)-1-(3-pyridyl)-1-butanol (NNAL) by the multidrug resistance protein 1 (MRP1): Requirement for glutathione or a non-sulfur-containing analog. J. Biol. Chem. 276, 27846–27854. https://doi.org/10.1074/jbc.M102453200.

Li, L., Liu, K.-H., Sheen, J., 2021. Dynamic nutrientsignaling networks in plants. Annu. Rev. Cell Dev. 37, 341–367. https://doi.org/10.1146/annurev-cellbio-010521-015047.

Li, W., Liu, Y., Liu, M., Zheng, Q., Li, B., Li, Z., Li, H., 2019. Sugar accumulationisassociated with leafsenescenceinduced by long-term high light in wheat. Plant Sci. 287, 110169. https://doi.org/10.1016/j.plantsci.2019.110169.

Lian, J., Liu, W., Meng, L., Wu, J., Chao, L., Zeb, A., Sun, Y., 2021. Foliar-appliedpolystyrenenanoplastics (PSNPs) reduce the growth and nutritionalquality of lettuce (Lactuca sativa L. EnvironmentalPollution 280, 116978. https://doi.org/10.1016/j.envpol.2021.116978.

Lian, J., Wu, J., Xiong, H., Zeb, A., Yang, T., Su, X., Su, L., Liu, W., 2020. Impact of polystyrenenanoplastics (PSNPs) on seedgermination and seedling growth of wheat (Triticumaestivum L.). J. Hazard. 385, 121620. https://doi.org/10.1016/j.jhazmat.2019.121620.

Lichtenthaler, H.K., 1987. Chlorophylls and carotenoids: pigments of photosyntheticbiomembranes. Methods Enzymol. 148, 350–382. https://doi.org/10.1016/0076-6879(87)48036-1.

Luo, H., Tu, C., He, D., Zhang, A., Sun, J., Li, J., Xu, J., Pan, X., 2023. Interactions betweenmicroplastics and contaminants: a review focusing on the effect of aging process. Sci. Total Environ. 899, 165615. https://doi.org/10.1016/j.scitotenv.2023.165615.

Mohana, A.A., Farhad, S.M., Haque, N., Pramanik, B.K., 2021. Understanding the fate of nano-plastics in wastewater treatment plants and theirremovalusing membrane processes. Chemosphere 284, 131430. https://doi.org/10.1016/j.chemosphere.2021.131430.

Murchie, E.H., Lawson, T., 2013. Chlorophyll fluorescence analysis: a guide to good practice and understanding some new applications. J. Exp. Bot. 64, 3983–3998. https://doi.org/10.1093/jxb/ert208.

Pizziconi, B., Bruno, G., Palombieri, S., Sestili, F., Cimini, S., De Gara, L., 2025. From soil to shoot plant responses to polystyrene nanoplastics and relevance for sustainable food systems. Plant Nanobiol., 100230 https://doi.org/10.1016/j.plana.2025.100230.

Saputra, F., Pramata, A.D., Soegianto, A., Hu, S.-Y., 2025a. Vitamin E mitigates polystyrene-nanoplastic- induced visual dysfunction in zebrafish larvae. Int. J. Mol. Sci. 26, 1216. https://doi.org/10.3390/ijms26031216.

Saputra, F., Tsao, Y.-T., Pramata, A.D., Soegianto, A., Hu, S.-Y., 2025b. Developmental cardiovascular disruption triggered by polystyrene nanoplastics in zebrafish mediated through oxidative stress. Life Sci 382, 124056. https://doi.org/10.1016/j.lfs.2025.124056.

Saputra, F., Tsao, Y.-T., Pramata, A.D., Soegianto, A., Hu, S.-Y., 2025c. Polystyrene nanoplastics act as endocrine disruptors altering neurotransmitter levels and locomotor activity via estrogen receptor during early zebrafish development. Aquat. Toxicol. 286, 107468. https://doi.org/10.1016/j.aquatox.2025.107468.

Siddiqui, S.A., Singh, S., Bahmid, N.A., Shyu, D.J.H., Domínguez, R., Lorenzo, J.M., Pereira, J.A.M., Câmara, J.S., 2023. Polystyrenemicroplasticparticles in the food

chain: characteristics and toxicity – a review. Sci. Total Environ. 892, 164531. https://doi.org/10.1016/j.scitotenv.2023.164531.
Sobral, A.F., Cunha, A., Costa, I., Silva-Carvalho, M., Silva, R., Barbosa, D.J., 2025. Environmentalxenobiotics and epigeneticmodifications: implications for human health and disease. J. Xenobiotics 15, 118. https://doi.org/10.3390/jox15040118.
Spanò, C., Muccifora, S., Ruffini Castiglione, M., Bellani, L., Bottega, S., Giorgetti, L., 2022. Polystyrenenanoplasticsaffectseedgermination, cellbiology and physiology of rice seedlings in short-term treatments: evidence of theirinternalization and translocation. Plant Physiol. Biochem. 178, 32–43. https://doi.org/10.1016/j.plaphy.2022.01.031.
Su, D., Li, W., Zhang, Z., Cai, H., Zhang, L., Sun, Y., Liu, X., Tian, Z., 2024. Discrepancy of Growth Toxicity of Polystyrene Nanoplastics on Soybean (Glycine max) and Mung Bean (Vigna radiata). Toxics 12. https://doi.org/10.3390/toxics12020155.
Suleiman, U.F., Ibrahim, S., 2024. Health and environmental impact of xenobiotics in water quality evaluation: A review. ujmr 299–307. https://doi.org/10.47430/ujmr.2493.036.
Sun, X.-D., Yuan, X.-Z., Jia, Y., Feng, L.-J., Zhu, F.-P., Dong, S.-S., Liu, J., Kong, X., Tian, H., Duan, J.-L., Ding, Z., Wang, S.-G., Xing, B., 2020. Differentially charged nanoplastics demonstrate distinct accumulation in Arabidopsis thaliana. Nat. Nanotechnol. 15, 755–760. https://doi.org/10.1038/s41565-020-0707-4.
Vicidomini, C., Palumbo, R., Moccia, M., Roviello, G.N., 2024. Oxidative processes and xenobiotic metabolism in plants: mechanisms of defense and potential therapeutic implications. J. Xenobiotics 14, 1541–1569. https://doi.org/10.3390/jox14040084.
Wong, J.C., Li, X., Kuan, H.N., Chia, C.H., Jin, K.S., Ree, M., 2020. Quantitative structural analysis of polystyrene nanoparticles using synchrotron x-ray scattering and dynamic light scattering. Plant Nanobiol. 12 (2), 477. https://doi.org/10.3390/polym12020477.
Xiao, F., Feng, L.-J., Sun, X.-D., Wang, Y., Wang, Z.-W., Zhu, F.-P., Yuan, X.-Z., 2022. Do Polystyrene Nanoplastics Have Similar Effects on Duckweed (Lemna minor L.) at Environmentally Relevant and Observed-Effect Concentrations? Environ. Sci. Technol. 56, 4071–4079. https://doi.org/10.1021/acs.est.1c06595.
Yan, S., Zhan, M., Liu, Z., Zhang, X., 2025. Insight into the transcriptional regulation of key genes involved in proline metabolism in plants under osmotic stress. Biochimie 228, 8–14. https://doi.org/10.1016/j.biochi.2024.08.006.
Zhang, Ya, Qiao, D., Zhang, Z., Li, Y., Shi, S., Yang, Y., 2024. Calcium signal regulated carbohydrate metabolism in wheat seedlings under salinity stress. Physiol. Mol. Biol. Plants 30, 123–136. https://doi.org/10.1007/s12298-024-01413-0.
Zhang, Y., Yang, X., Luo, Z.-X., Lai, J.-L., Li, C., Luo, X.-G., 2022. Effects of polystyrene nanoplastics (PSNPs) on the physiology and molecular metabolism of corn (Zea mays L.) seedlings. Sci. Total Environ. 806, 150895. https://doi.org/10.1016/j.scitotenv.2021.150895.
Zhou, C.-Q., Lu, C.-H., Mai, L., Bao, L.-J., Liu, L.-Y., Zeng, E.Y., 2021. Response of rice (Oryza sativa L.) roots to nanoplastic treatment at seedling stage. J. Hazard. Mater. 401, 123412. https://doi.org/10.1016/j.jhazmat.2020.123412.
Zhou, Q., Lian, J., Liu, W., Men, S., Wu, J., Sun, Y., Zeb, A., Yang, T., Ma, Q.,2020. Transcriptome mechanisms underlying interaction of polystyrene nanoplastics and wheat Triticum aestivum L. https://doi.org/10.21203/rs.3.rs-98748/v1.